Fermi National Accelerator Laboratory

FN-368
2562.000
LBL-14587
(Submitted to
Nucl. Instr. and Methods)

SATURATED AVALANCHE CALORIMETER*

M. Atac
Fermi National Accelerator Laboratory, Batavia, Illinois 60510 USA

S. Kim
Tsukuba University, Ibaraki, Japan

M. Mishina
National Laboratory for High Energy Physics (KEK), Tsukuba, Japan

W. Chinowsky, R. Ely, M. Gold, J. Kadyk, P. Rowson, K. Shinsky, and Y. Wang†
Lawrence Berkeley Laboratory, Berkeley, California 94720 USA

R. Morse and M. Procario
University of Wisconsin, Madison, Wisconsin 53706 USA

and

T. Schaad
Harvard University, Cambridge, Massachusetts 02138 USA

April 1982

Abstract

A gas sampling electromagnetic calorimeter running in a "Saturated Avalanche Mode" was tested at SLAC with positrons incident at energy up to 17.5 GeV. With this new method, good energy resolution, 16 percent/$\sqrt{E}$, and good linearity were obtained[1] with arrays of thirty-four 0.5 radiation length thick lead plates interleaved with 34 wire counters. There was no measurable systematic effect. Amplifiers are not needed; the signals are large enough to be connected directly to the ADC's.

*Supported in part by the Director, Office of Energy Research, Office of Basic Energy Sciences, Chemical Sciences Division of the U. S. Department of Energy under Contract No. DE-AC03- 76SF00098.
†Present address: Institute of HEP, Ac. Sinica, Beijing, P. R. China.

Introduction

Gas sampling calorimeters operating in a proportional mode have been tested and used by several groups[2-11] but, with one reported exception[7], their energy resolution has been much inferior to that achieved with calorimeters that use plastic scintillator counters. Improved resolution for energy less than 5 GeV has been demonstrated in a calorimeter operated in the Geiger mode[12], and may be expected also with the limited streamer[13,14] mode. Those devices are intrinsically different from proportional counter energy sampling calorimeters. The former, in effect, use the number of tracks in the shower, while the latter use the magnitude of total collected charges as measures of the energy deposited in the gas. In this paper, we report results of tests of gas sampling calorimeters run in neither of these modes, but in an intermediate, partially saturated mode. Their resolution is comparable to that of plastic scintillator calorimeters.

These tests were made as part of the program to develop calorimeter modules for the Collider Detector Facility[15], an apparatus to detect products of $\bar{p}p$ interactions at the 2 TeV colliding beams machine now under construction at Fermilab. The present design (Fig. 1) calls for gas sampling electromagnetic and hadronic calorimetry in the forward and backward angular regions. Respectably small granularity will be achieved with tower structures of cathode readout pads.

Experimental Arrangements

Two detectors studied were a MAC prototype[7] and brass tube calorimeter[11], which were tested previously in proportional mode at SLAC and at Fermilab, respectively. Thus, only limited details of construction will be given here.

The MAC prototype was composed of 34 lead plates of 2.8 mm thickness and 34 planes of 50 μm diameter anode wires enclosed in 9.5 mm x 9.5 mm cells which are separated by 1.5 mm thick aluminum ribs, a 17.8 radiation length shower detector. Fig. 2 shows the arrangement and the cell structure. Both detectors were individually placed in aluminum containers which could be evacuated or pressurized for studying pressure effects. The anode wires of each plane were connected to a common strip, and seven such planes were further grouped together, resulting in five groups to be read out. Results will be presented based on data obtained from the total sum of these five groups as well as from the individual sections to show the longitudinal development of the shower.

The counter gas was a mixture of 49.3 percent Argon, 49.3 percent ethane, and 1.4 percent ethyl alcohol. Negative high voltage was applied to the cathode tubes. Distributed high voltage capacitors totaling 0.25 μf were the charge storage elements. As indicated in the figure, there was no need for amplifiers between the wires and the ADC's. Indeed, it was necessary to attenuate the large signals obtained between 2 db and 30 db depending on the high voltage and gas pressure. Coaxial cables of 40 m length carried the signals to the LeCroy 2249W ADC's. The gate width was 1.2 μsec.

The wires of the brass tube calorimeter were connected together longitudinally, as shown in Fig. 3, and further grouped as indicated above and in

the figure. This calorimeter is made of 0.36 mm wall thickness, 6.3 mm x 11.3 mm cross section brass tubes containing 50 μm diameter anode wires. Forty 2 mm thick lead plates were between the wire planes to give a total of 16.5 radiation lengths.

A LSI-11 computer system with a SLAC program package "ATROPOS" was used for data taking and on-line display and monitoring.

Beam Parameters

The detectors were tested in the 19^{o} beam of the Stanford Linear Accelerator which provided positrons of 17.5 GeV maximum energy. SLAC ran in the SLED mode during the entire tests with a bunch length of about 20 nsec, and 10 bunches per second. About 95 percent of the beam at the detector was within the 2 mm x 2 mm area of the beam defining counter. The average intensity was between 1/10 and 10 positrons per bunch. The momentum spread of the beam, $\Delta p/p$ was less than ±0.25 percent rms.

Experimental Results

Most of the data presented here were taken with the MAC prototype calorimeter. Gain and resolution were measured at various settings of gas pressure and applied voltage with positrons incident at selected energies in the range 1.5 GeV-17.5 GeV available in the SLAC test beam. A representative sample of results will be shown.

1. Shower sum

For 10 GeV incident positrons, the total pulse height distribution is shown in Fig. 4 together with a Gaussian fit to the data. Only that portion

within $\pm 2\sigma$ of the mean were used in the fitting procedure. The shape of the distribution, typical of all, is well represented by the Gaussian function.

With fixed gas pressure, the resolution σ/E varies with high voltage as shown in Fig. 5. As the voltage increases from 2100 V, the resolution slowly decreases to a shallow minimum at $\sim$ 2250 V and then slowly increases.

Figs. 6a and 6b present the calorimeter output as a function of incident positron energy. Both at 0 psig and 5 psig there are no detectable non-linearities at energies up to 17.5 GeV. For these runs, the counters were run at 2300 V and 2550 V, respectively.

Fig. 7 shows the total pulse height as a function of high voltage for the pressures of 0 psig and 3 psig. Both show approximately exponential rise in gain with increasing voltage. The higher pressure curve has some indication of an inflection point near the middle of the range.

Higher energy response of the detector was simulated by using multiple positrons in a single rf bucket. This is a fair simulation since the positive ions do not move appreciably from where they were produced during the beam spill. Fig. 8 shows the detector response to multiple positrons of 17.5 GeV. It shows that as many as 11 simultaneous positrons the energy resolution of the detector is sufficiently good to resolve them with clear minima between the peaks of the pulse height distributions for the corresponding numbers of positrons. In fact, this is a Poisson distribution for $n = 4.5$. The oscilloscope trace reproduced in Fig. 9 shows some pulses for single and double positrons. The pulse rise time is about 10 nsec, and the decay time is almost 800 nsec. The decay time is long because the whole detector whose capacitance exceeds 10 nF was connected to a single 50 Ω coaxial cable. The pulse height

for singles is $\sim$ 75 mV and is $\sim$ 150 mV for doubles. These pulses can be used for a prompt multiplicity trigger with a time jitter of few nanoseconds. The pulse heights for the multiple positrons deviate in a smooth way from linear behavior for more than a two-positron (35 GeV) shower, as seen in Figs. 10a and 10b. The linearity is much better at 8 psig. The ADC pedestals were determined by extrapolating to zero energy the line determined by the first two points in each plot. An expanded view of the pulse height distribution for 10 GeV positrons is shown in Fig. 11. It dramatically shows the symmetric, Gaussian-like shapes with clean valleys between the multiple-hit peaks. The energy resolution as a function of equivalent energy deposits of multiple 17.5 GeV positrons is shown in Fig. 12 after correction for the nonlinear response.

The energy resolution as a function of energy for single incident positrons is shown in Fig. 13. σ/E shows the usual $E^{-1/2}$ dependence with a constant factor of 16.2 percent as indicated in Fig. 14. The fact that the resolution extrapolates to the origin indicates that there are no systematic effects. This is, perhaps, because there is no active device (amplifier, pulse shaper, etc.) between the detector and the ADC, and small variations among individual wire gains average out over the detector.

The detector was rotated to make angles to the beam axis of as much as 23°, with 17.5 GeV positrons incident, the results of Fig. 15 were obtained. It is seen that the pulse height increases by a small amount (maximum 2.3 percent), and the σ/E decreases slightly with increasing angle. This improvement may be due to a better containment of energy in the increased thickness of the rotated calorimeter.

Similar results were obtained from the brass tube calorimeter. It was run only at 6 psig pressure. Fig. 16 shows that the energy resolution is almost 17 percent/$\sqrt{E}$ and independent of high voltage, in contrast to the behavior of the MAC prototype. The reason for the differences between the two may be the different cell shapes. It is curious that poorer resolution was found with the thinner lead sampling sheets. When the brass tube calorimeter was tested at Fermilab in the proportional mode, the resolution was measured to be 22 percent/$\sqrt{E}$.

2. Shower development

The response of each of the five 3.3 radiation length thick sections of the MAC detector is plotted in Figs. 17a-17e (see Fig. 8 for an example of the sum signal). These show pulse height distributions obtained with multiple 17.5 GeV positrons incident on the detector operated at 3.0 psig gas pressure and 2.40 kV applied voltage. Only in the center section is the resolution sufficient to separate the peaks due to different numbers of positrons in single beam bunches. The pulse height distributions, correpsonding to a particular number of positrons were determined for each of the five sections by selecting events whose total recorded pulse height (summed over five sections) is within the limits appropriate to a selected positron multiplicity. Figs. 18a-18e show scatter plots of each of the five distributions vs. the sum of the outputs of the five ADC's. Distinct clusters of data points are clearly seen in each plot, showing the response to as many as 13 positrons simutaneously incident on the calorimeter segments. In Fig. 19 we show the mean pulse heights as a function of the number of positrons. Comparison of the measured pulse height values with those indicated by the straight lines gives

a measure of the non-linearity vs. energy. For example, with 105 GeV of energy incident on the calorimeter these are in segments 1 through 5, 14.5 percent, 14.8 percent, 9.3 percent, 2.4 percent, and 0.5 percent, respectively. In the sum of these signals, it is 9.6 percent. Note that the deviation from linearity is substantial in the first segment, where the deposited energy is smallest. In section 5, which has comparable energy deposit, little saturation can be seen. The deviation in section 2 is considerably greater than in section 3 which has approximately the same energy deposit. This behavior appears to indicate a saturation effect that depends on the density of particles within the shower.

The pattern of energy deposited in the gas of the calorimeter as a function of the shower depth is demonstrated in Fig. 20, where we show the mean pulse height from each section as a function of position. The data for energies less than 17.5 GeV have been corrected to account for gain variation due to small pressure changes that occurred during the runs. Results are shown at several energies between 2.0 GeV and 17.5 GeV. For comparison, energy deposits inferred from the universal shower curves of Abshire et al.[16] have been superimposed, and the agreement is seen to be good. The position of the shower median as a function of depth is shown in Fig. 21, together with a curve inferred from the universal function of Abshire et al. Again, there is good agreement.

Saturated Avalanche Mode

We have investigated the ionization region[13] between the proportional region and the self quenching streamer region in detail using a 9 mm x 9.5 mm

tube having a 50 μm wire, a replica of one cell of the prototype MAC detector, in order to understand the dependence of the energy resolution on high voltage.

A small fraction of the wire pulse was amplified and used to form the ADC trigger, as shown in Fig. 22. A LeCroy 2285 ADC system was used for measuring the charge. The gain of the ADC was 20 counts per picocoulomb. An Fe^{55} x-ray source was used to measure the wire gain as a function of high voltage. As seen in Figs. 23a and 23b, the resolution is insufficient to separate the 5.9 keV x-ray line and 2.9 keV argon escape line when the gas gain, at 2300 V, is the region of limited proportionality. The gain here was $\sim 5 \times 10^4$. The 2.9 keV line is hidden in the left side of the asymmetric pulse height distribution. Fig. 24 shows the gain as a function of the high voltage. The rate of growth of the avalanche is seen to decrease continuously as the high voltage increases above 2200 V until the streamer threshold is reached. Then the gain increases very little to the point of full streamer operation around 2650 V.

The distribution of pulse heights recorded by passage of minimum ionization tracks was also investigated in this voltage region using a Sr^{90} β-source. A telescope made from a pair of small thin scintillation counters provided a gate pulse for the ADC's. The discriminator thresholds were set to accept mainly the minimum ionizing β's. Fig. 25a shows the pulse height distribution obtained at 2300 V. This histogram shows that the distribution is almost symmetric with a small tail. The distribution made by the β's is not like the typical Landau distribution, shown in Fig. 25b, obtained in a gas gap of 9.5 mm thickness, at 1800 volts, and atmospheric pressure. Comparison of this distribution with that of Fig. 25a shows that the tail is greatly suppressed at the higher voltage. Landau fluctuations clearly have been reduced,

an indication that the greater the concentration of primary ionization, the more saturation (less gain) occurs, as has been observed earlier.[17]

From the data of Fig. 23, we find a ratio of mean pulse heights produced by the two photons of $\sim$ 1.4, rather than the $\sim$ 2.0 ratio of energies. Similar conclusions about the departure from strict linear, proportional response follows from comparison of the signals from the β and x-ray sources. Those observations and the suppression of the Landau tail indicate partial saturation of the avalanche charge at the collecting wire. Thus, the energy resolution is improved compared to that generally obtained when the counters operate in the proportional mode. We find a resolution somewhat smaller than, but not really inconsistent with that predicted by Fischer[18], which is based on a calculation of the response without the effect of Landau fluctuations. Deterioration in resolution at voltages much higher than 2400 V may be caused by fluctuations in gain where streamer and saturated avalanche modes overlap (see Fig. 24). Depending on the amount of ionization deposited locally on the wire, the gain may be low (saturated avalanche) or more than an order of magnitude higher (streamer).

Acknowledgments

The authors express their appreciation to R. Coombes, R. Prepost, and D. M. Ritson for providing the MAC prototype; to R. Schwitters and A. Tollestrup for support; to R. Gearhart and the SLAC operating crew for assisting and supporting the runs; to P. Clancy and S. Mackenzie for help with the data acquisition system; and to M. Hrycyk for modifying the brass-tube calorimeter.

References

Ref. 1 Preliminary results were reported at the 2nd Topical Conference on Forward Collider Physics, Madison, Wisconsin (December 1981).

Ref. 2 W. Murzin, Progr. Element. Part. Cosmic Ray Phys. 245 (1967).

Ref. 3 M. E. Nordberg, Jr., Cornell Univ. Report, CLNS 138 (1971).

Ref. 4 T. Katsura et al., Nucl. Instr. and Meth. 105, 245 (1972).

Ref. 5 M. Atac, IEEE Trans. on Nucl. Sci., Vol. NS-28, No. 1, 492 (Feb. 1981).

Ref. 6 M. Atac et al., IEEE Trans. on Nucl. Sci., Vol. NS-28, No. 1, 500 (Feb. 1981).

Ref. 7 R. L. Anderson et al., IEEE Trans. on Nucl. Sci., Vol. NS-25, 340 (1978).

Ref. 8 C. Bosio et al., Nucl. Instr. and Meth. 157, 35 (1978).

Ref. 9 P. Skubic et al., IEEE Trans. on Nucl. Sci., Vol. NS-28, No. 1, 496 (Feb. 1981).

Ref. 10 H. Ticho et al., UCLA Report.

Ref. 11 M. Mishina et al., private communication.

Ref. 12 W. Carithers et al., private communication; to be published in Nucl. Instr. and Meth.

Ref. 13 M. Atac et al., Fermilab Report FN-337 (1981), and Proc. of INS International Symp. on Nucl. Radiation Detectors, 327 (March 1981), Tokyo. University of Tokyo publication.

Ref. 14 M. Jonker et al., Physica Scripta, 23, 677 (1981).

Ref. 15 Fermilab $\bar{p}p$ Colliding Detector Proposal (1979).

Ref. 16 G. Abshire et al., NIM 164, 67 (1979).

Ref. 17 H. Frehse et al., Nucl. Instr. and Meth. 156, 87 (1978).

Ref. 18 G. Fischer, Nucl. Instr. and Meth. 156, 81 (1978).

Figure Captions

Fig. 1 — A cross section view of the Collider Detector Facility at Fermilab.

Fig. 2 — The experimental configuration of the MAC electromagnetic calorimeter.

Fig. 3 — The experimental configuration of the brass tube electromagnetic calorimeter.

Fig. 4 — A typical pulse height distribution and Gaussian fitted points for obtaining σ and mean values using 2σ fit.

Fig. 5 — σ/E vs. high voltage for 10 GeV positrons at 0 psig.

Fig. 6a-b — The total pulse height response of the calorimeter as function of the e energy for 0 psig and 5 psig, respectively. The linearity is excellent for both pressures.

Fig. 7 — The total pulse height as a function of the high voltage for pressures of 0 psig and 3 psig.

Fig. 8 — The response of the detector to simultaneous multiple positrons of 17.5 GeV.

Fig. 9 — The oscilloscope picture of some single and double 17.5 GeV positron pulses.

Fig. 10a-b — The pulse heights as a function of simultaneous 17.5 GeV multiple positrons for 0 psig and 8 psig.

Fig. 11 — Pulse height distributions for 10 GeV multiple positrons.

Fig. 12 — $\sigma/\sqrt{E}$ vs. simultaneous multiple 17.5 GeV positrons after correction for non-linear response.

Fig. 13 — σ/E vs. positron energy.

Fig. 14 — σ/E vs. $E^{-1/2}$.

Fig. 15 — Total pulse height and σ/E vs. incident beam angle for 17.5 GeV positrons.

Fig. 16 — $\sigma/\sqrt{E}$ vs. the high voltage for the brass tube calorimeter.

Fig. 17a-e — Pulse height distributions in each 3.3 radiation length segments of the calorimeter with incident multiple 17.5 GeV positrons.

Fig. 18a-e Scatter plots of pulse heights in each section vs. the sum of the five outputs.

Fig. 19 Mean pulse height vs. the number of incident positrons for each segment. The straight lines are determined by the first two points.

Fig. 20 Mean pulse height in a calorimeter segment vs. positron in depth. The form of the superimposed curve is discussed in the text.

Fig. 21 Position of shower maximum as a function of energy.

Fig. 22 The circuit diagram for investigating the saturation avalanche region.

Fig. 23a-b Pulse height distributions for the 5.9 x-rays from Fe^{55}. Fig. 23a shows the ADC distribution without amplifier. Note the 3 keV argon escape line is not visible in the saturated avalanche because of poor proportionality. Fig. 23b shows the amplified distribution where the escape line is just visible because of the better resolution at high pulse heights.

Fig. 24 The model tube gain as a function of the high voltage in the saturated avalanche region using the ADC without amplifier.

Fig. 25a The pulse height distribution for minimum ionizing tracks in the saturated avalanche region showing almost symmetric distribution with very small Landau tail. (HV = 2300 volts)

Fig. 25b As 24a at 1800 volts, showing a distribution with its Landau tail. A low gain amplifier was used for obtaining this distribution.

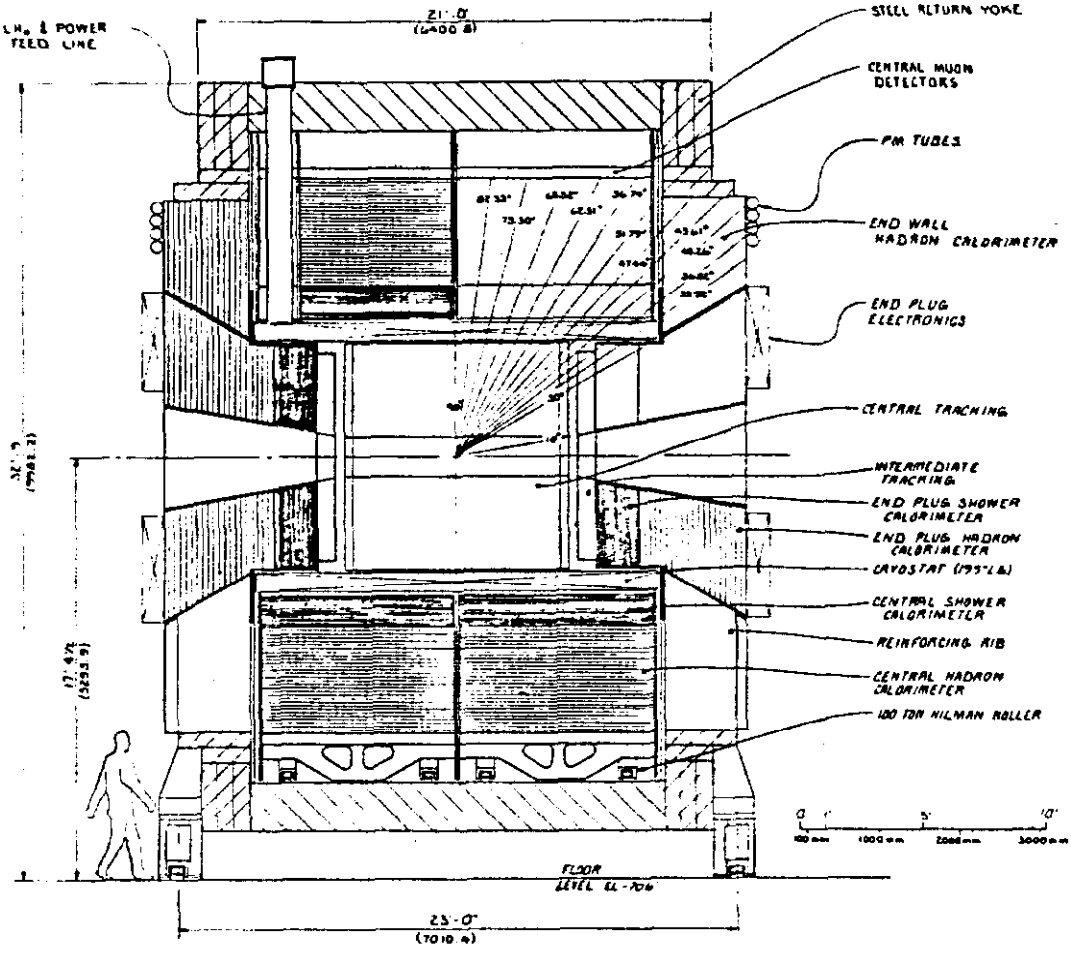
STEEL RETURN YOKE
CENTRAL MUON DETECTORS
PM TUBES
END WALL HADRON CALORIMETER
END PLUG ELECTRONICS
CENTRAL TRACKING
INTERMEDIATE TRACKING
END PLUG SHOWER CALORIMETER
END PLUG HADRON CALORIMETER
CRYOSTAT
CENTRAL SHOWER CALORIMETER
REINFORCING RIB
CENTRAL HADRON CALORIMETER
100 TON HILMAN ROLLER
FLOOR

Fig. 1

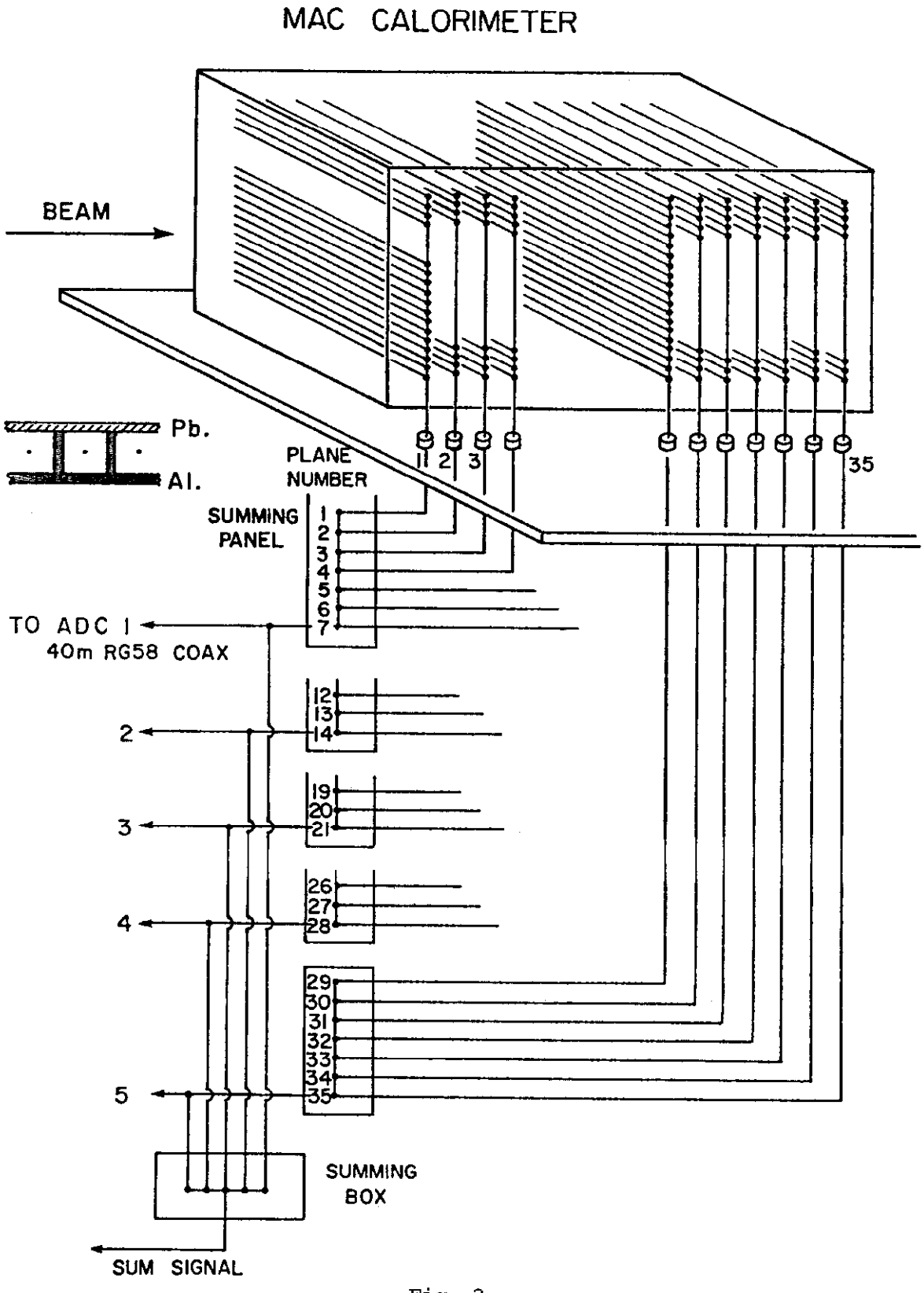
MAC CALORIMETER
BEAM
Pb.
Al.
PLANE NUMBER
1 2 3
35
SUMMING PANEL
1
2
3
4
5
6
7
TO ADC 1
40m RG58 COAX
12
13
14
2
19
20
21
3
26
27
28
4
29
30
31
32
33
34
35
5
SUMMING BOX
SUM SIGNAL

Fig. 2

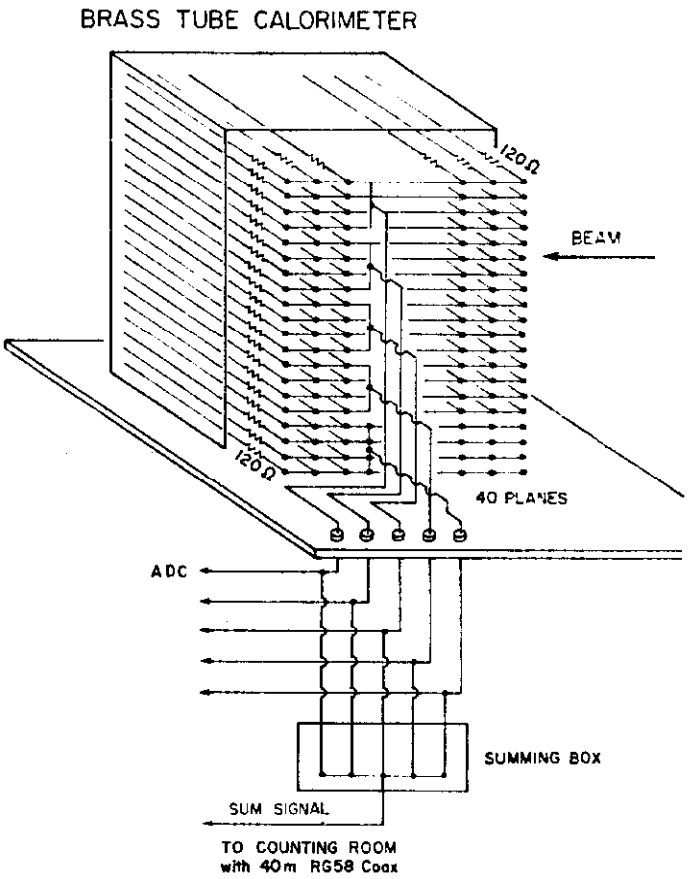
BRASS TUBE CALORIMETER
120Ω
BEAM
120Ω
40 PLANES
ADC
SUMMING BOX
SUM SIGNAL
TO COUNTING ROOM
with 40m RG58 Coax

Fig. 3

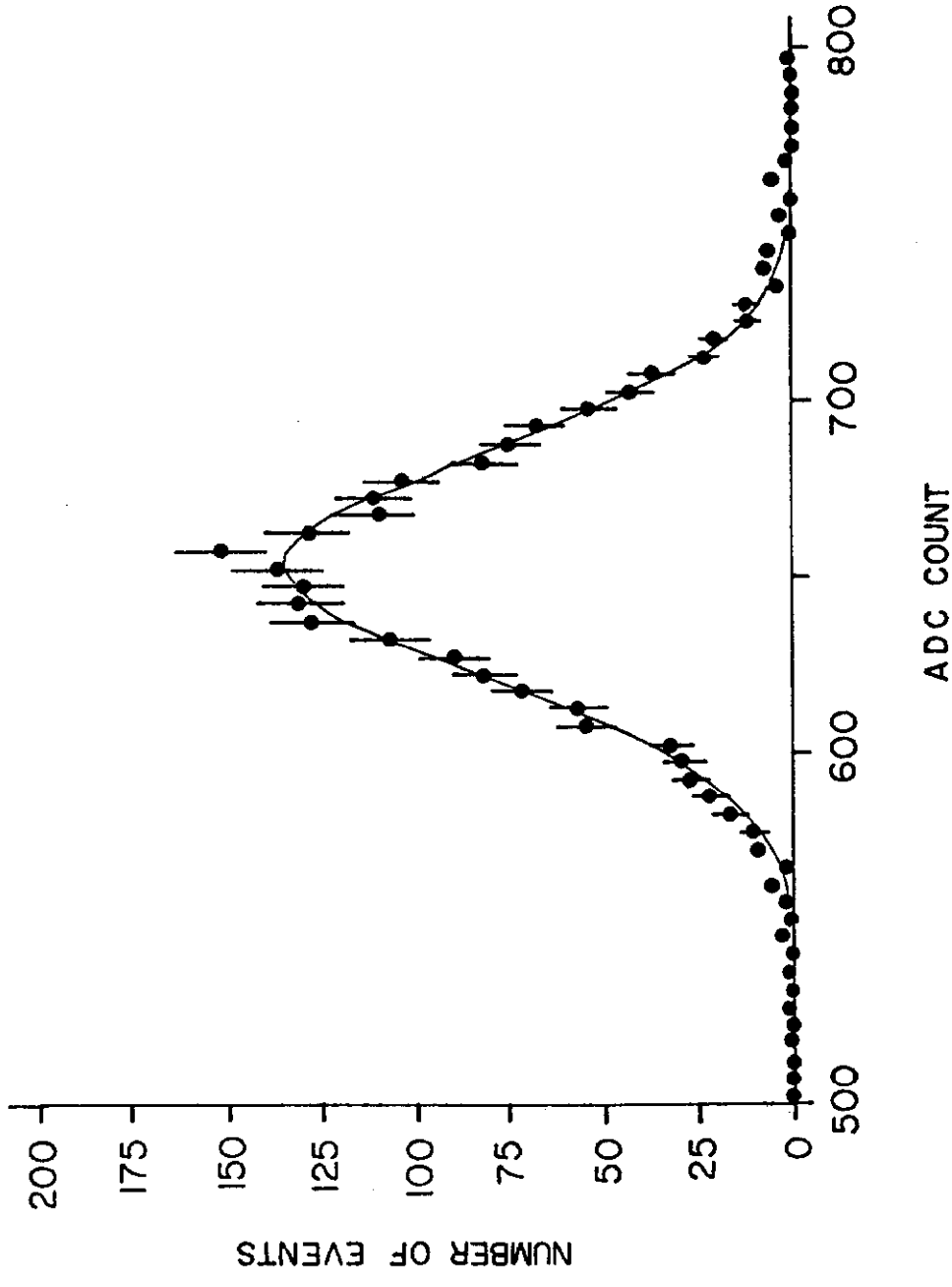
NUMBER OF EVENTS
200
175
150
125
100
75
50
25
0
500
600
700
800
ADC COUNT

Fig. 4

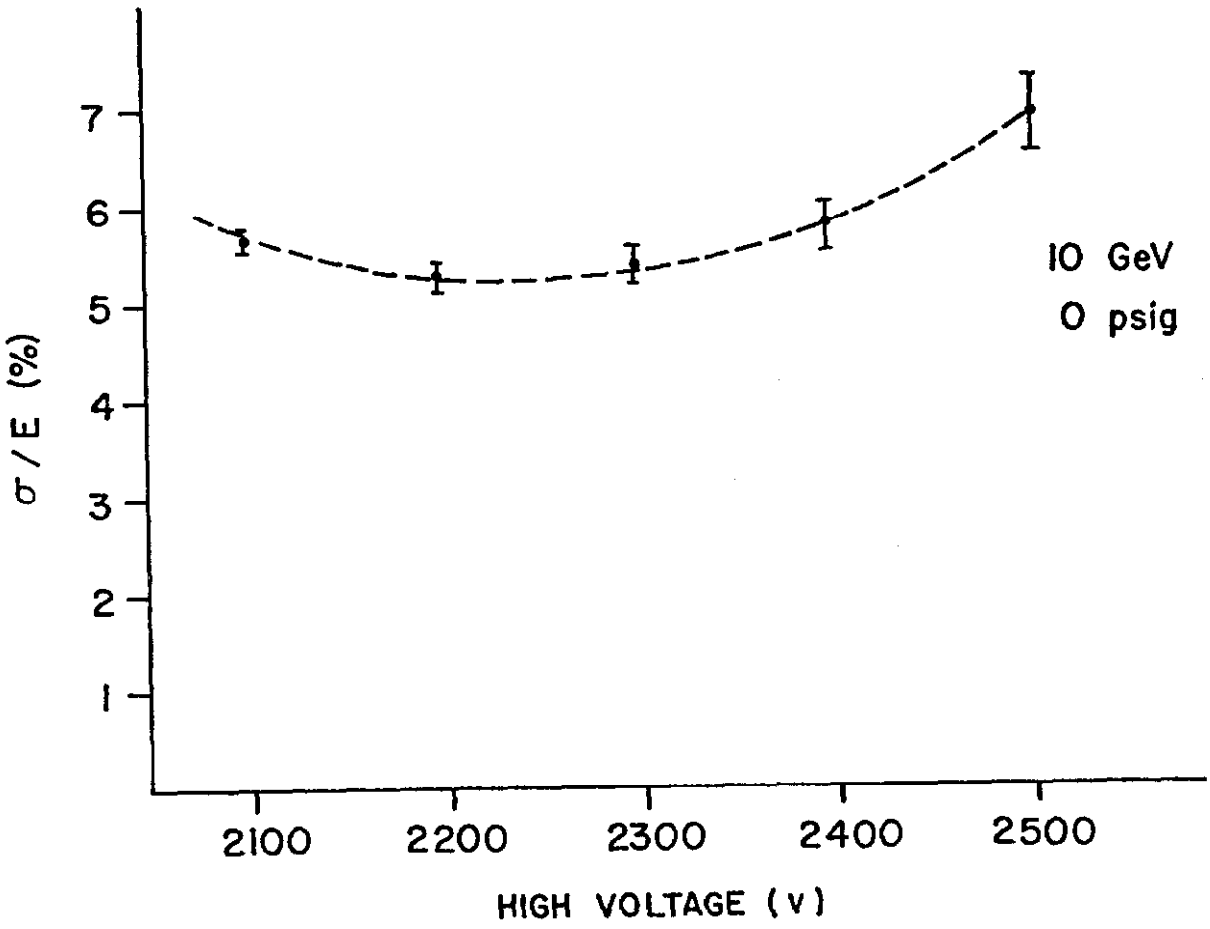
σ / E (%)
7
6
5
4
3
2
1
2100
2200
2300
2400
2500
HIGH VOLTAGE (V)
10 GeV
0 psig

Fig. 5

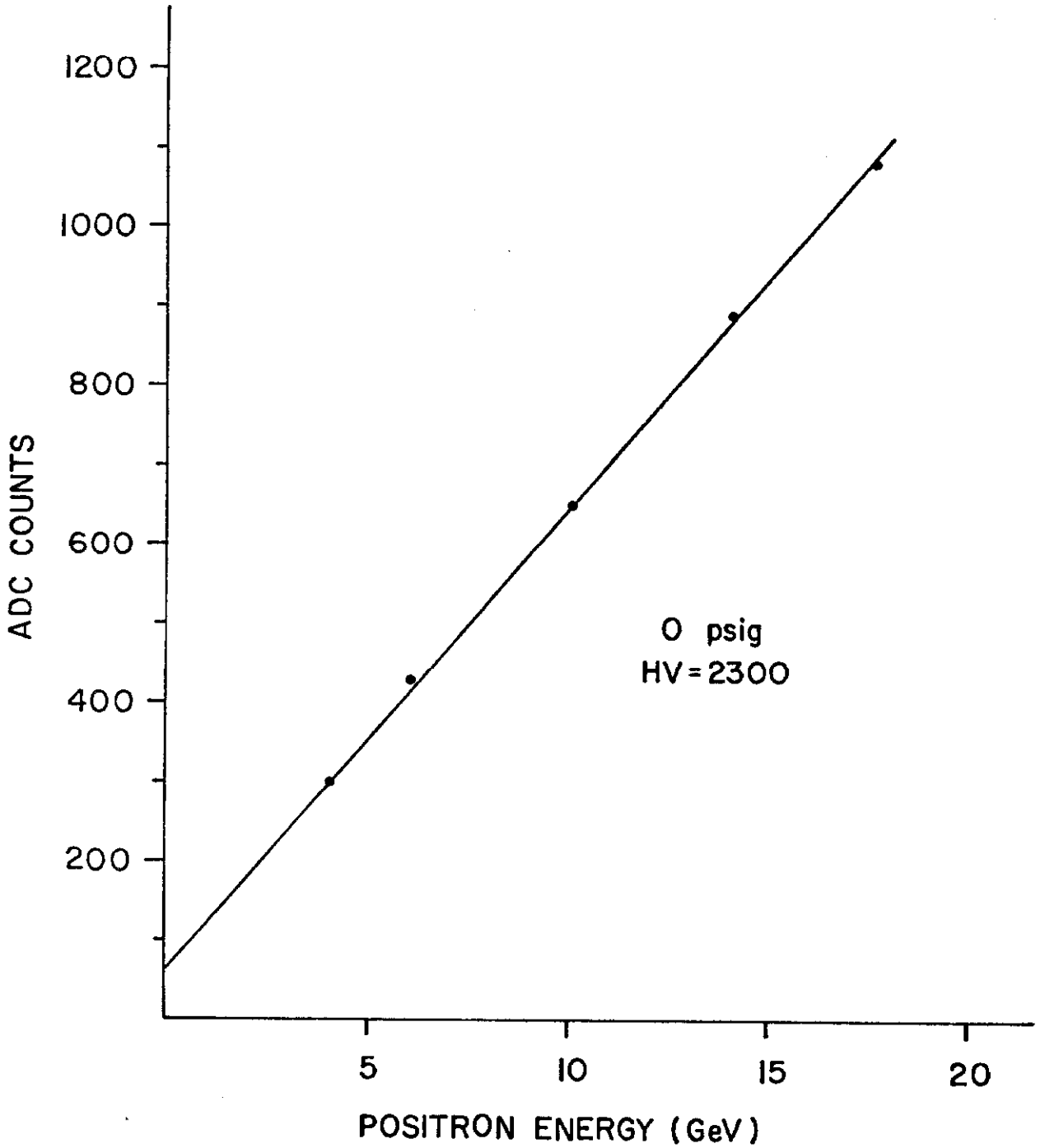
1200
1000
800
600
400
200
ADC COUNTS
0 psig
HV = 2300
5
10
15
20
POSITRON ENERGY (GeV)

Fig. 6a

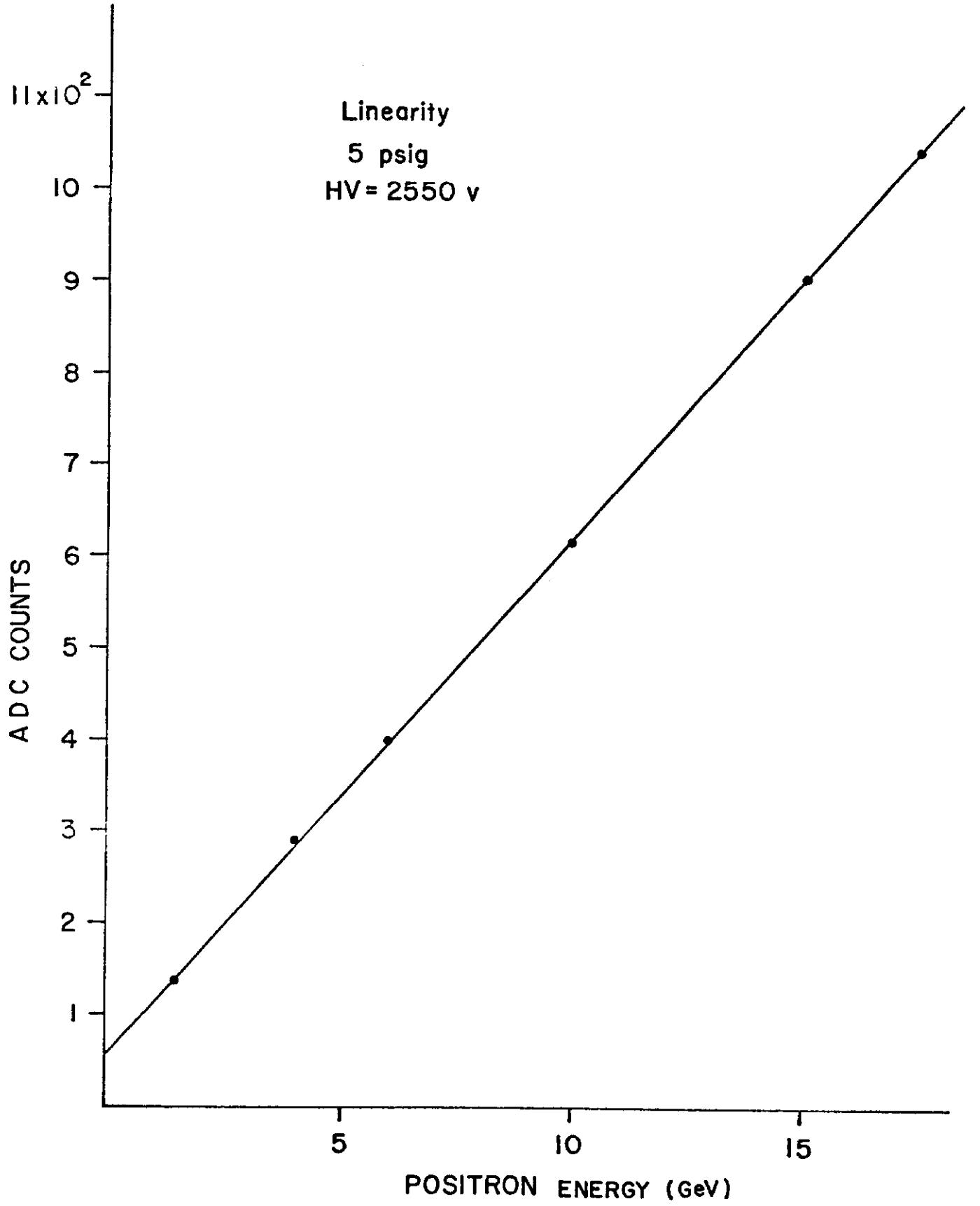
Linearity
5 psig
HV = 2550 v
11x10²
10
9
8
7
6
5
4
3
2
1
ADC COUNTS
5
10
15
POSITRON ENERGY (GeV)

Fig. 6b

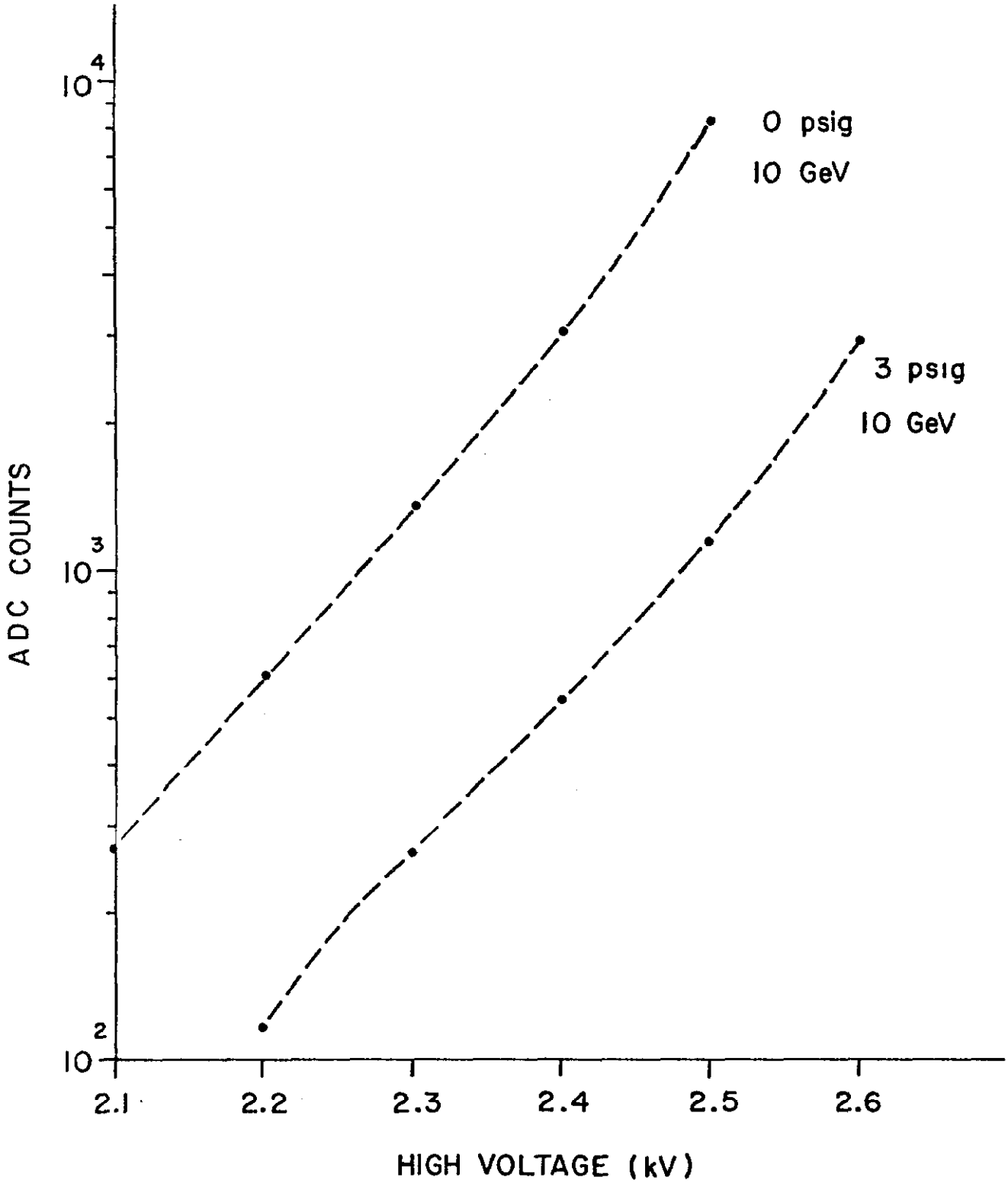
ADC COUNTS
10^4
10^3
10^2
2.1
2.2
2.3
2.4
2.5
2.6
HIGH VOLTAGE (kV)
0 psig
10 GeV
3 psig
10 GeV

Fig. 7

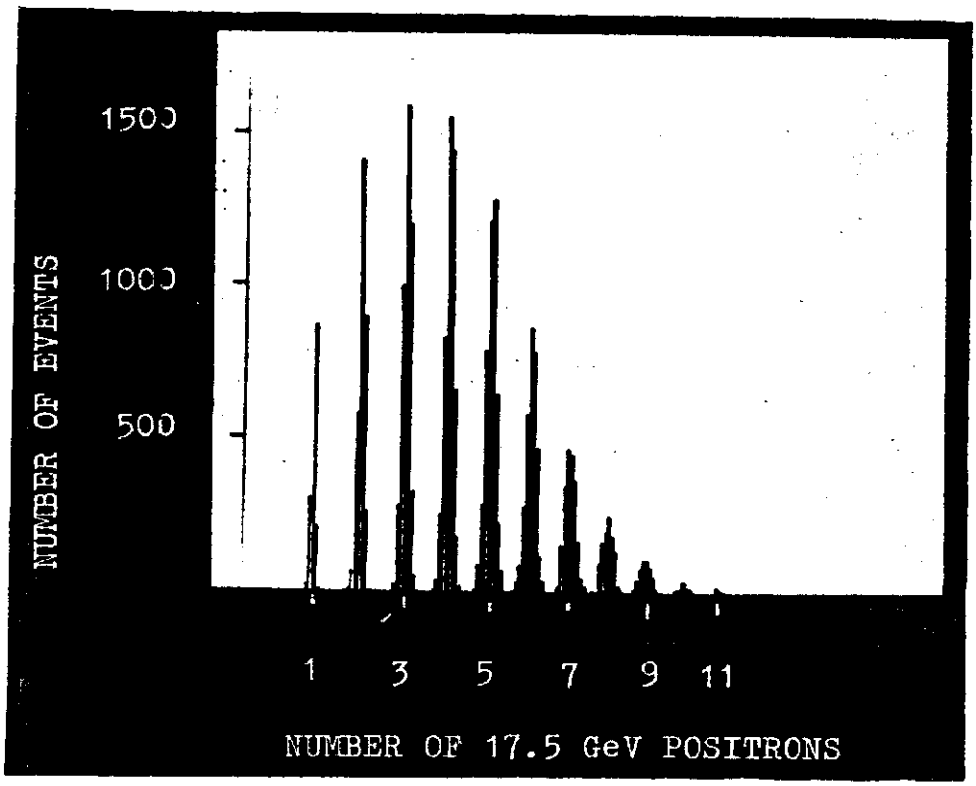
1500
1000
500
NUMBER OF EVENTS
1
3
5
7
9
11
NUMBER OF 17.5 GeV POSITRONS

Fig. 8

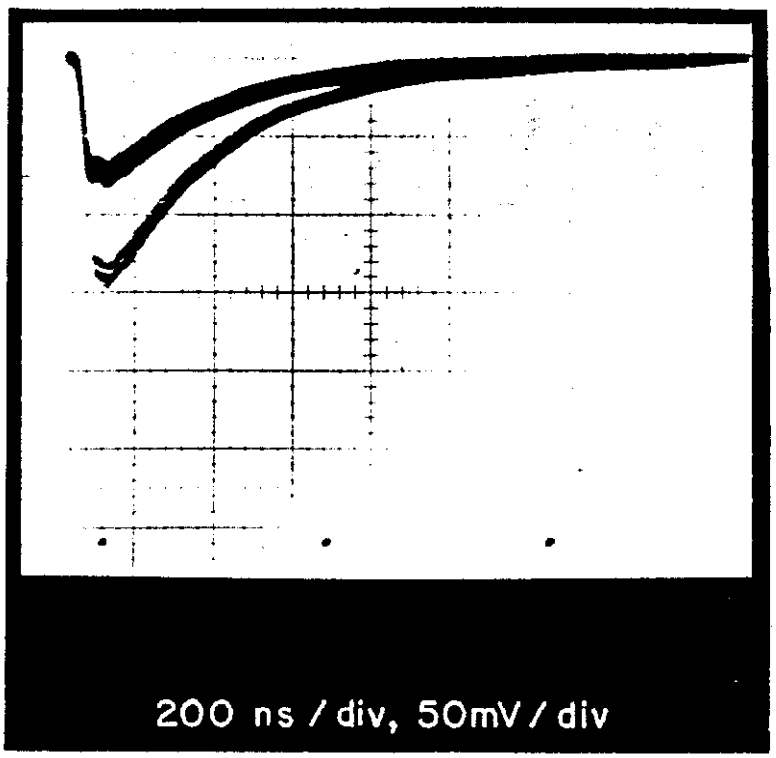

Fig. 9

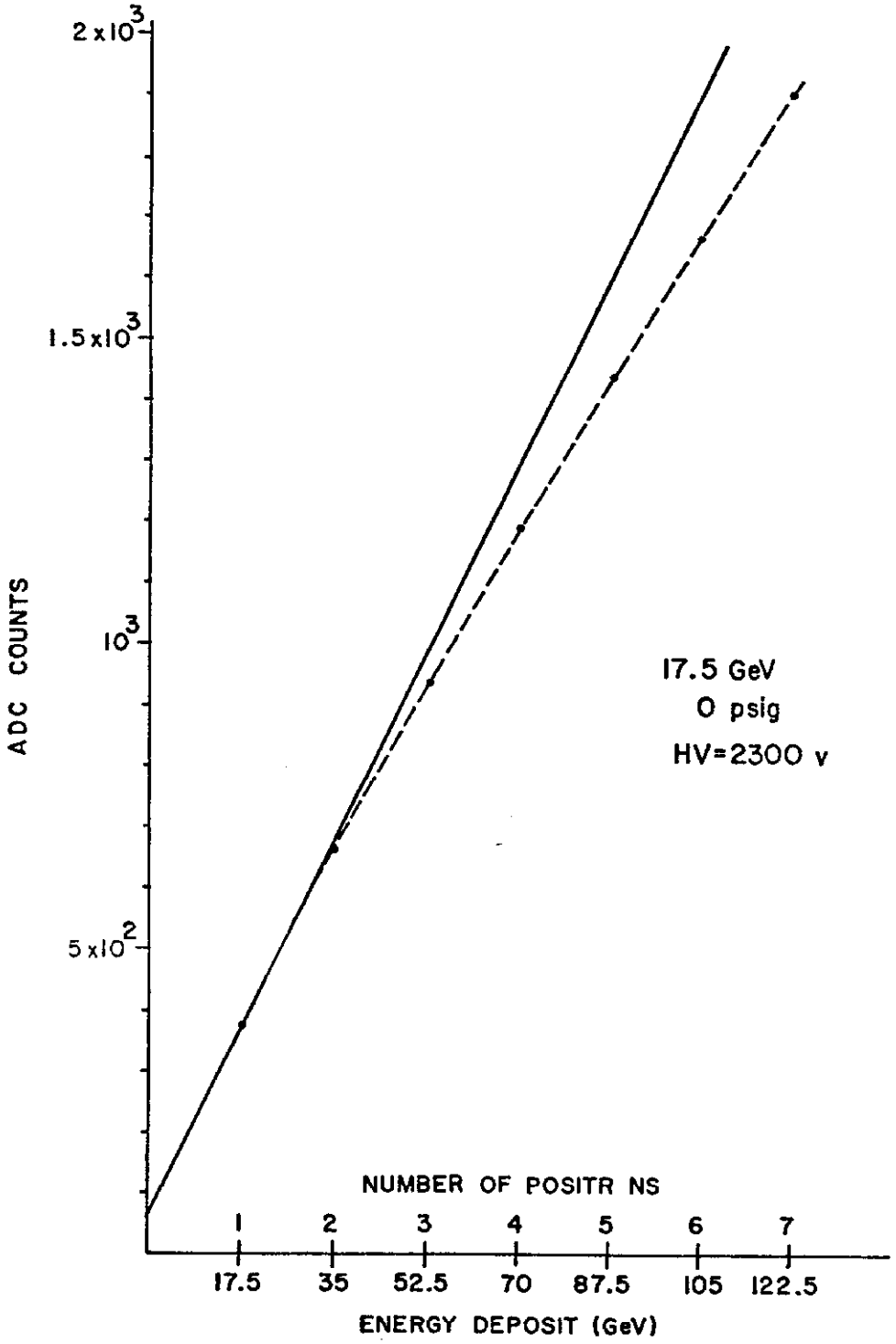
2x10^3
1.5x10^3
10^3
5x10^2
ADC COUNTS
17.5 GeV
0 psig
HV=2300 v
NUMBER OF POSITR NS
1
2
3
4
5
6
7
17.5
35
52.5
70
87.5
105
122.5
ENERGY DEPOSIT (GeV)

Fig. 10a

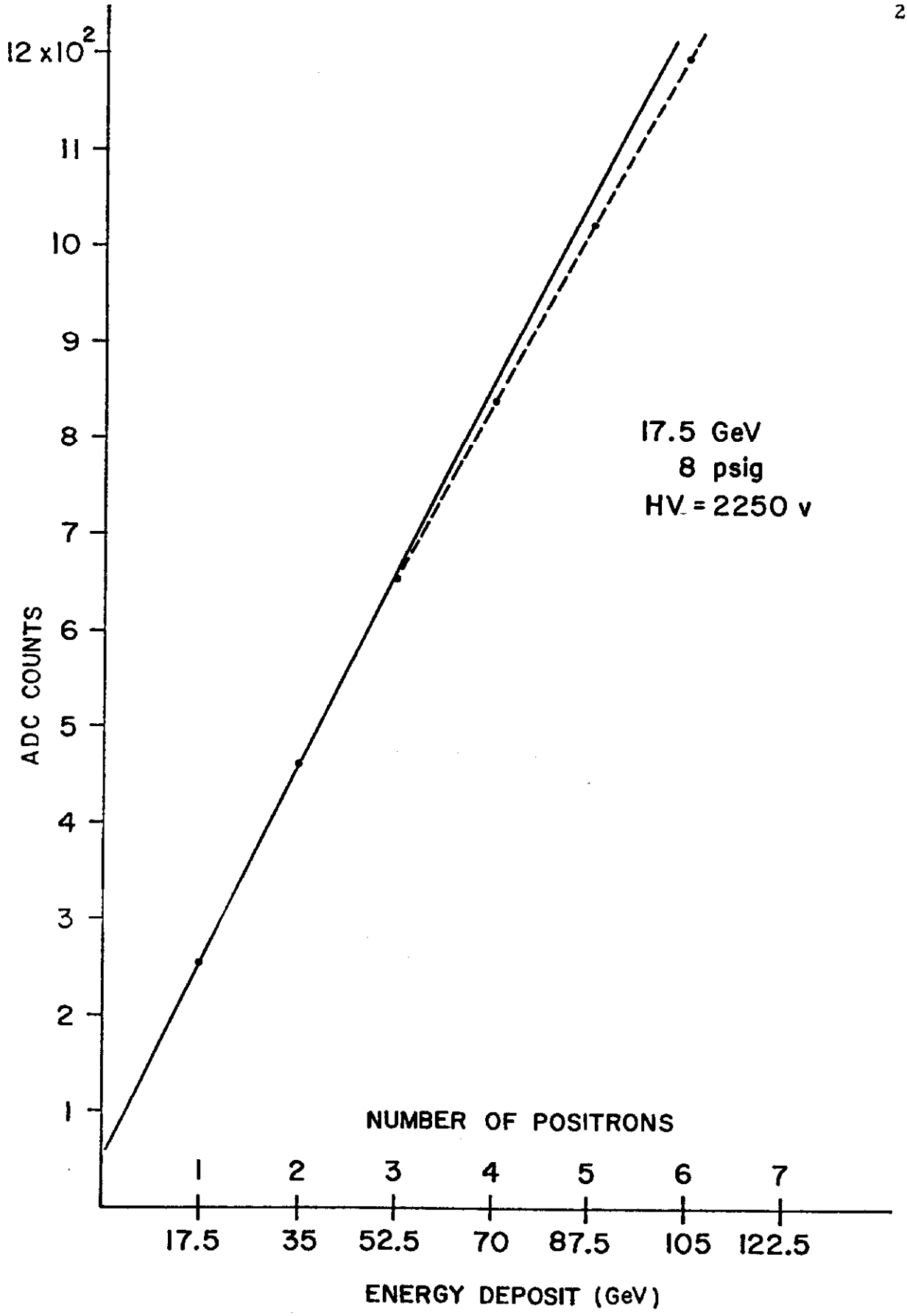
12 x10²
11
10
9
8
7
6
5
4
3
2
1
ADC COUNTS
17.5 GeV
8 psig
HV = 2250 v
NUMBER OF POSITRONS
1
2
3
4
5
6
7
17.5
35
52.5
70
87.5
105
122.5
ENERGY DEPOSIT (GeV)

Fig. 10b

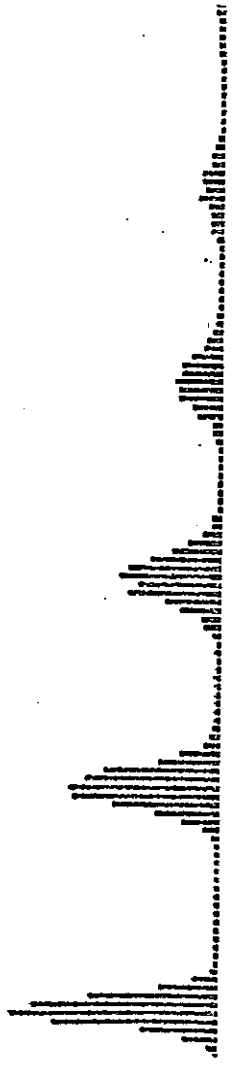

Fig. 11

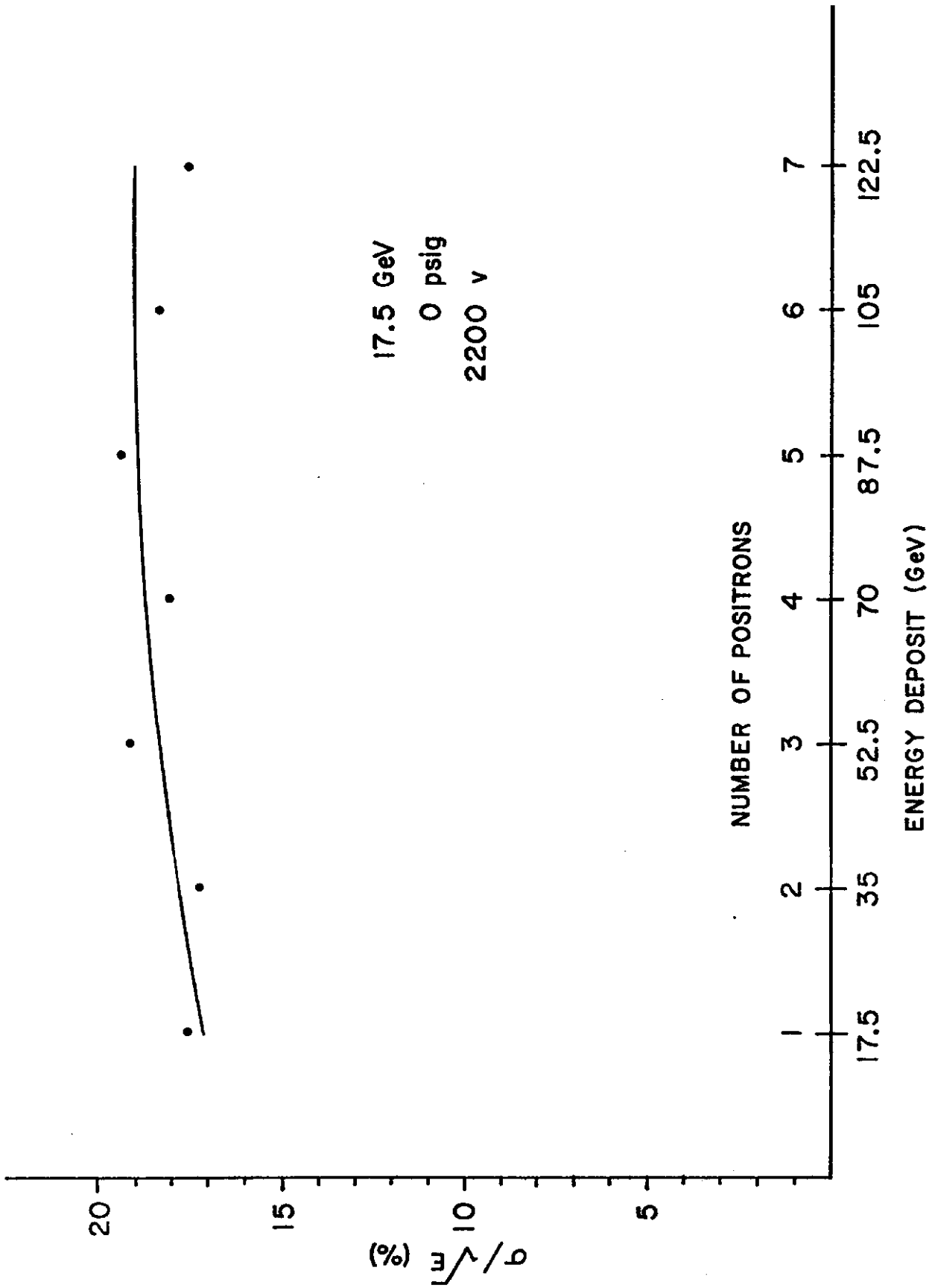
17.5 GeV
0 psig
2200 v
σ/√E (%)
20
15
10
5
NUMBER OF POSITRONS
1
2
3
4
5
6
7
ENERGY DEPOSIT (GeV)
17.5
35
52.5
70
87.5
105
122.5

Fig. 12

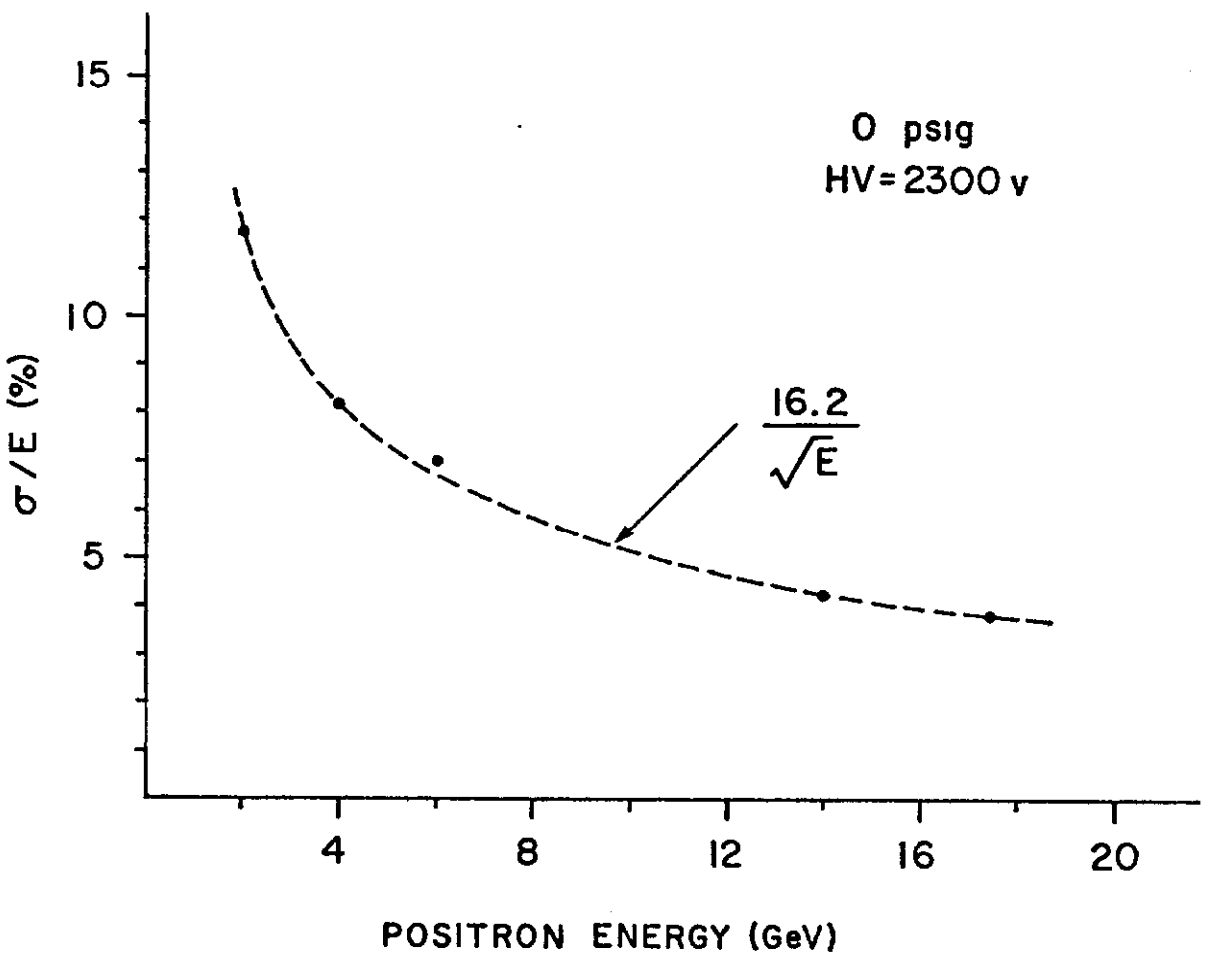

Fig. 13

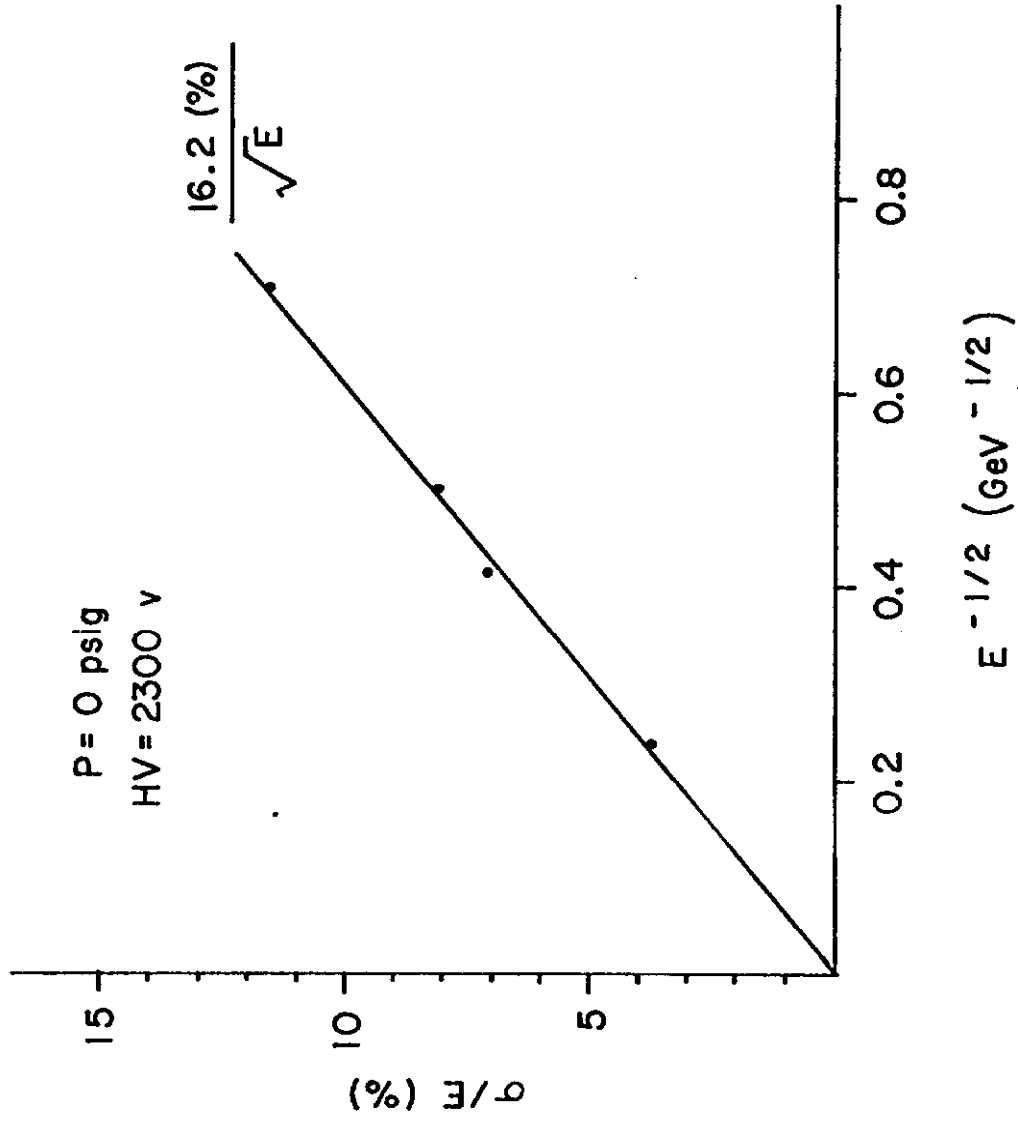

Fig. 14

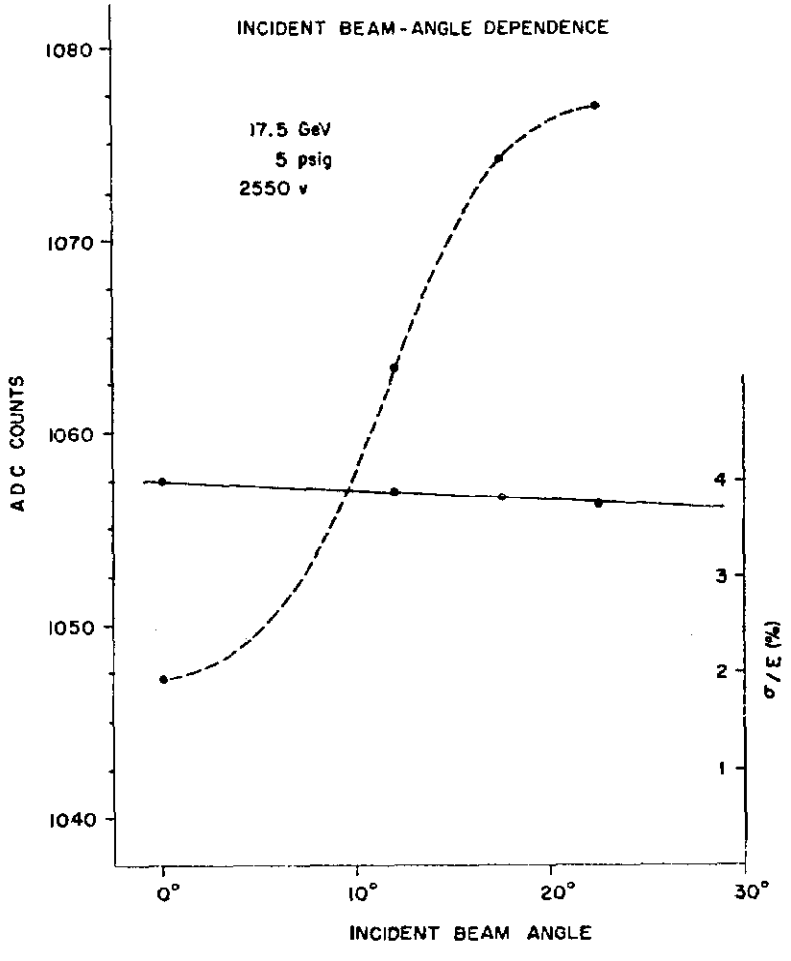
INCIDENT BEAM-ANGLE DEPENDENCE
17.5 GeV
5 psig
2550 v
ADC COUNTS
1080
1070
1060
1050
1040
4
3
2
1
σ/E (%)
0°
10°
20°
30°
INCIDENT BEAM ANGLE

Fig. 15

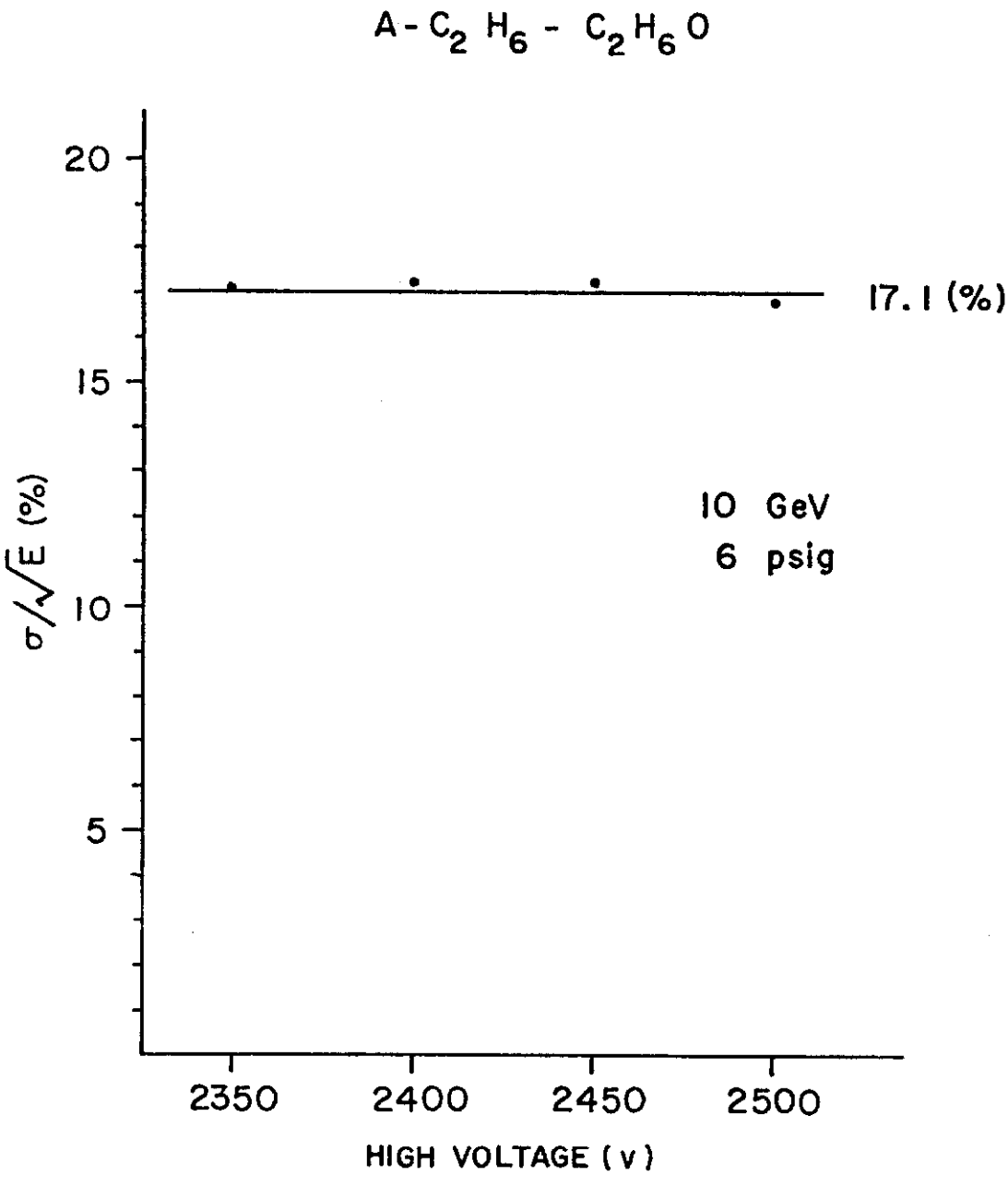
A - $C_2 H_6$ - $C_2 H_6 O$
20
15
10
5
$\sigma/\sqrt{E}$ (%)
17.1 (%)
10 GeV
6 psig
2350
2400
2450
2500
HIGH VOLTAGE (v)

Fig. 16

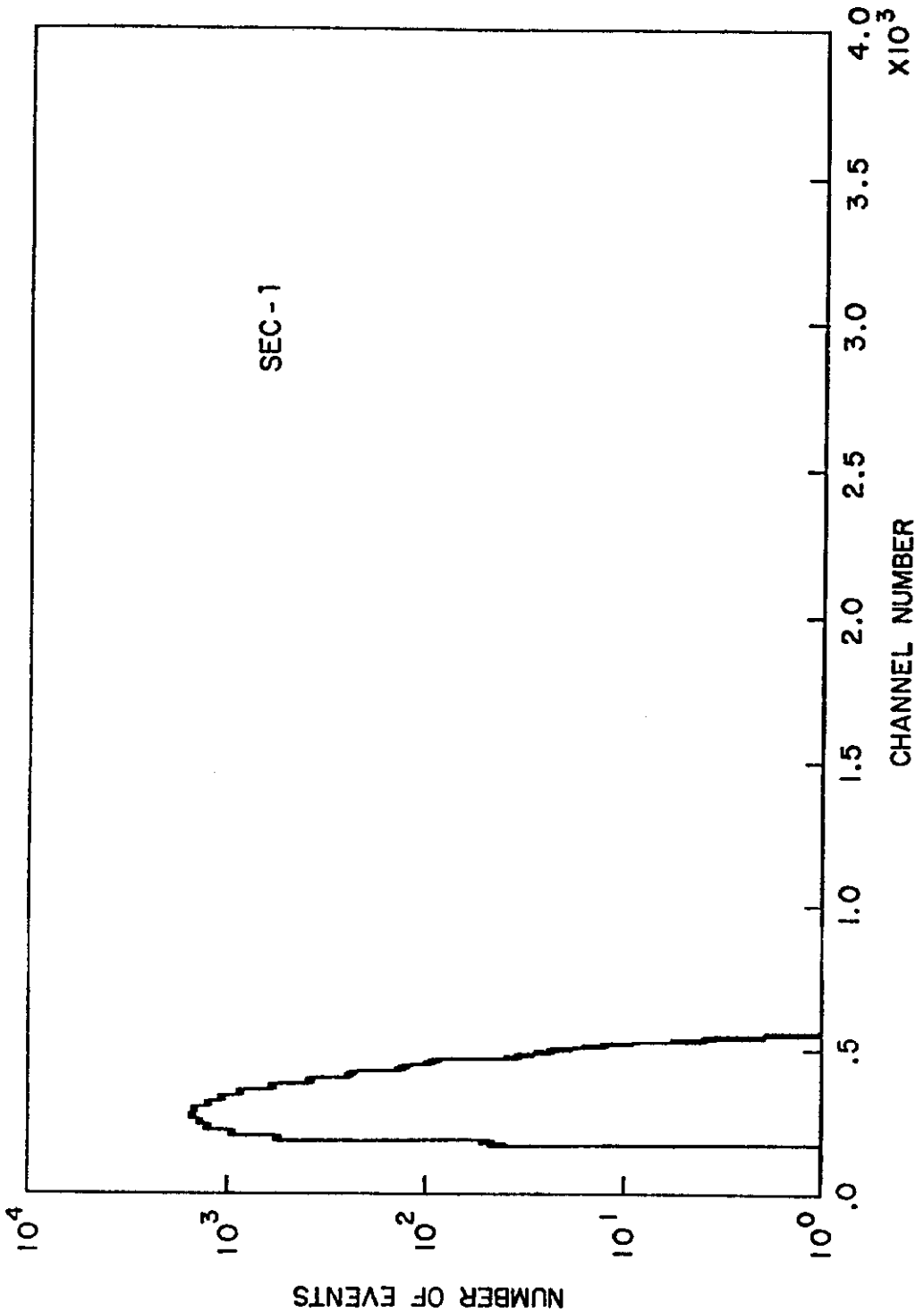
SEC-1
NUMBER OF EVENTS
10^4
10^3
10^2
10^1
10^0
.0
.5
1.0
1.5
2.0
2.5
3.0
3.5
4.0
X10^3
CHANNEL NUMBER

Fig. 17a

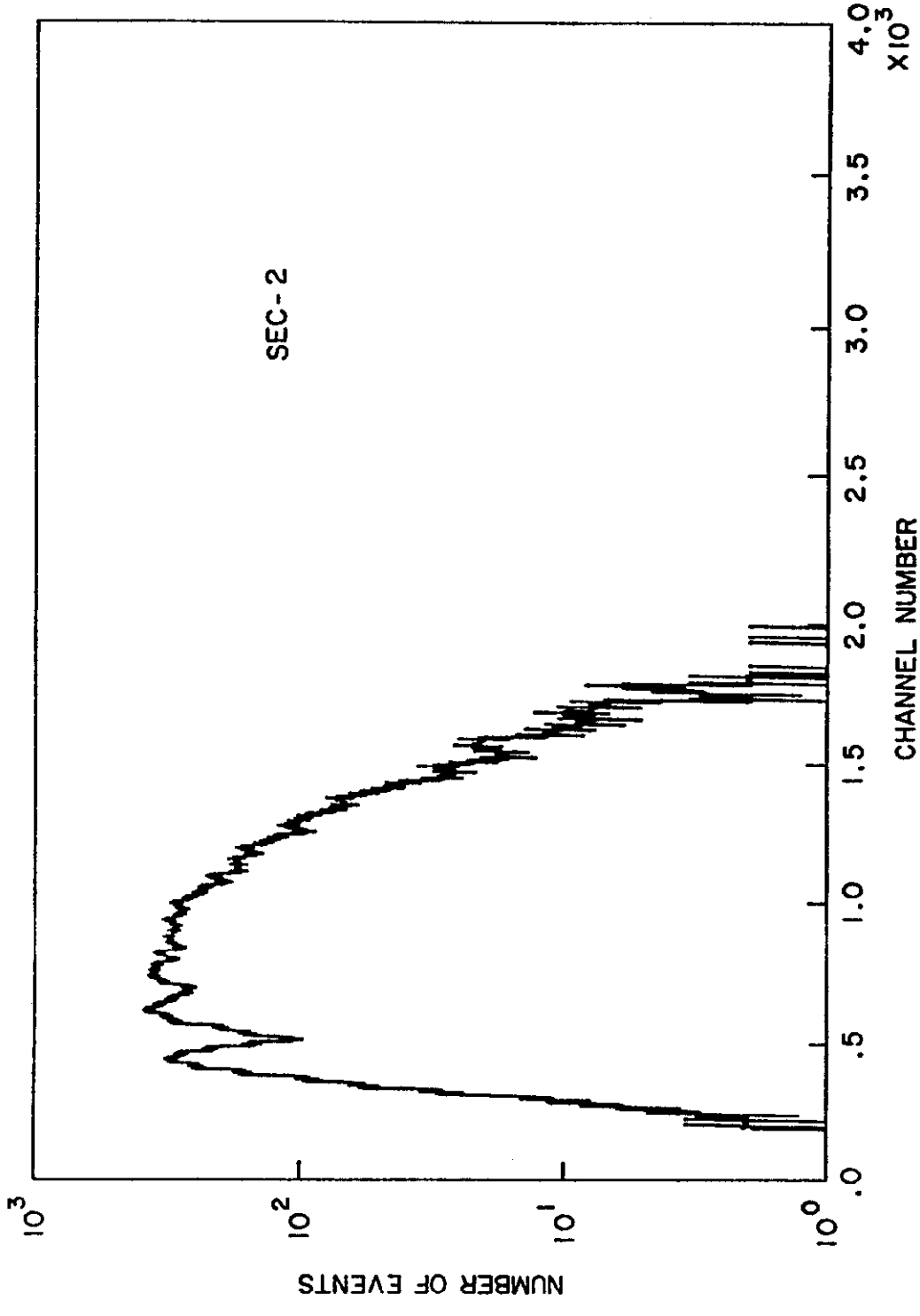
SEC-2
NUMBER OF EVENTS
CHANNEL NUMBER
X10^3
10^0
10^1
10^2
10^3
.0
.5
1.0
1.5
2.0
2.5
3.0
3.5
4.0

Fig. 17b

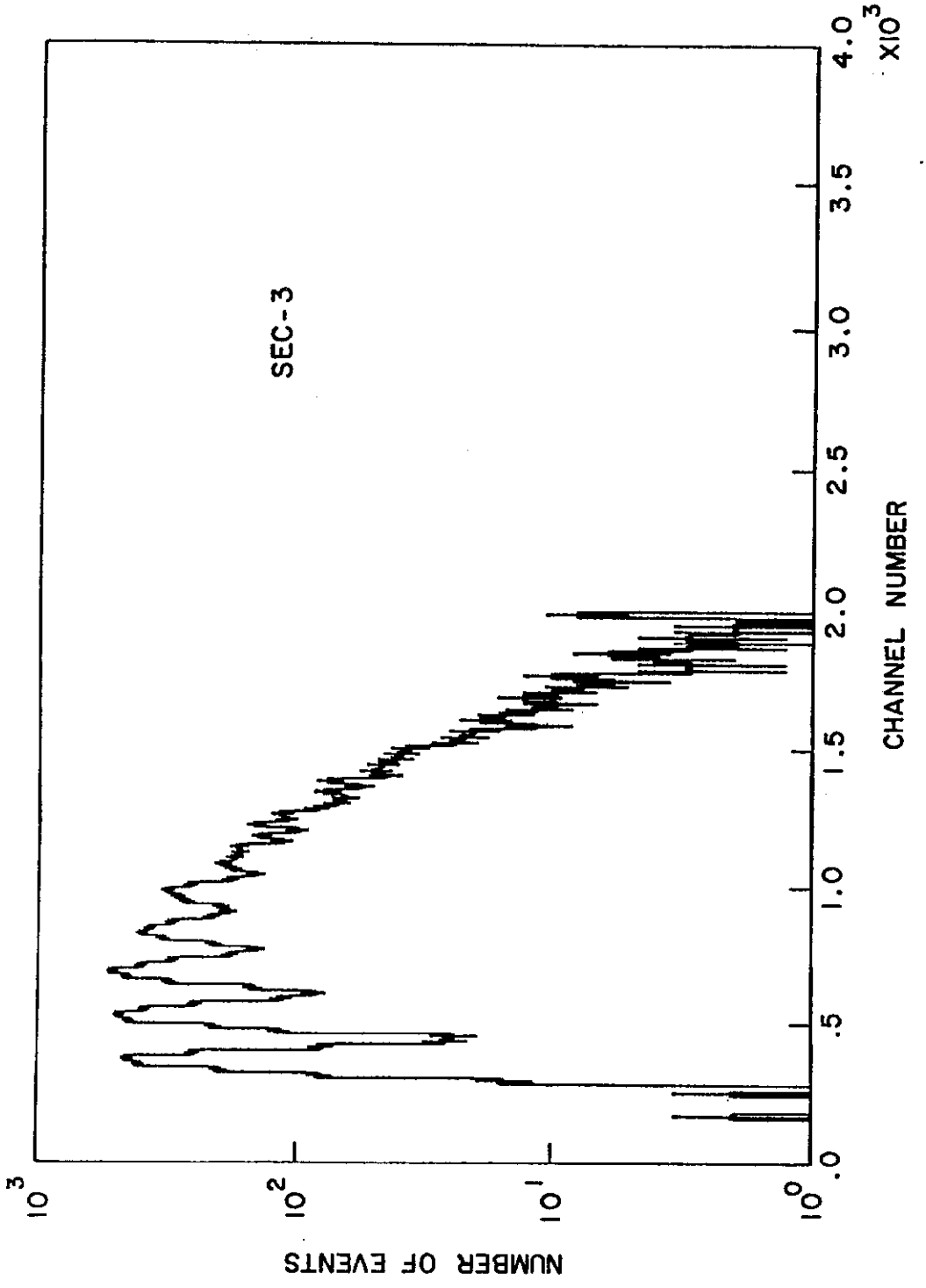
SEC-3
NUMBER OF EVENTS
CHANNEL NUMBER
X10^3
10^3
10^2
10^1
10^0
.0
.5
1.0
1.5
2.0
2.5
3.0
3.5
4.0

Fig. 17c

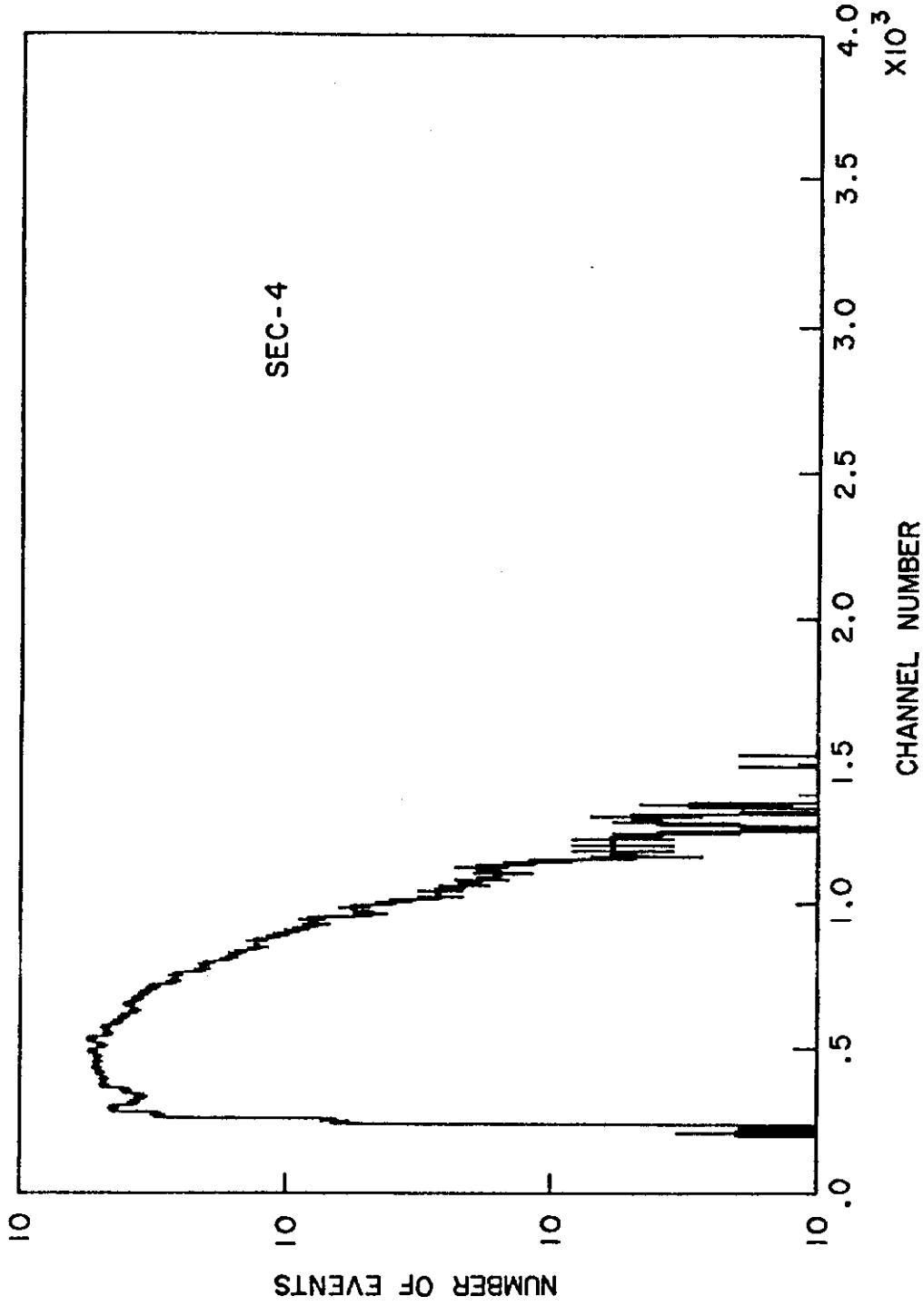
SEC-4
NUMBER OF EVENTS
CHANNEL NUMBER
X10³
.0
.5
1.0
1.5
2.0
2.5
3.0
3.5
4.0

Fig. 17d

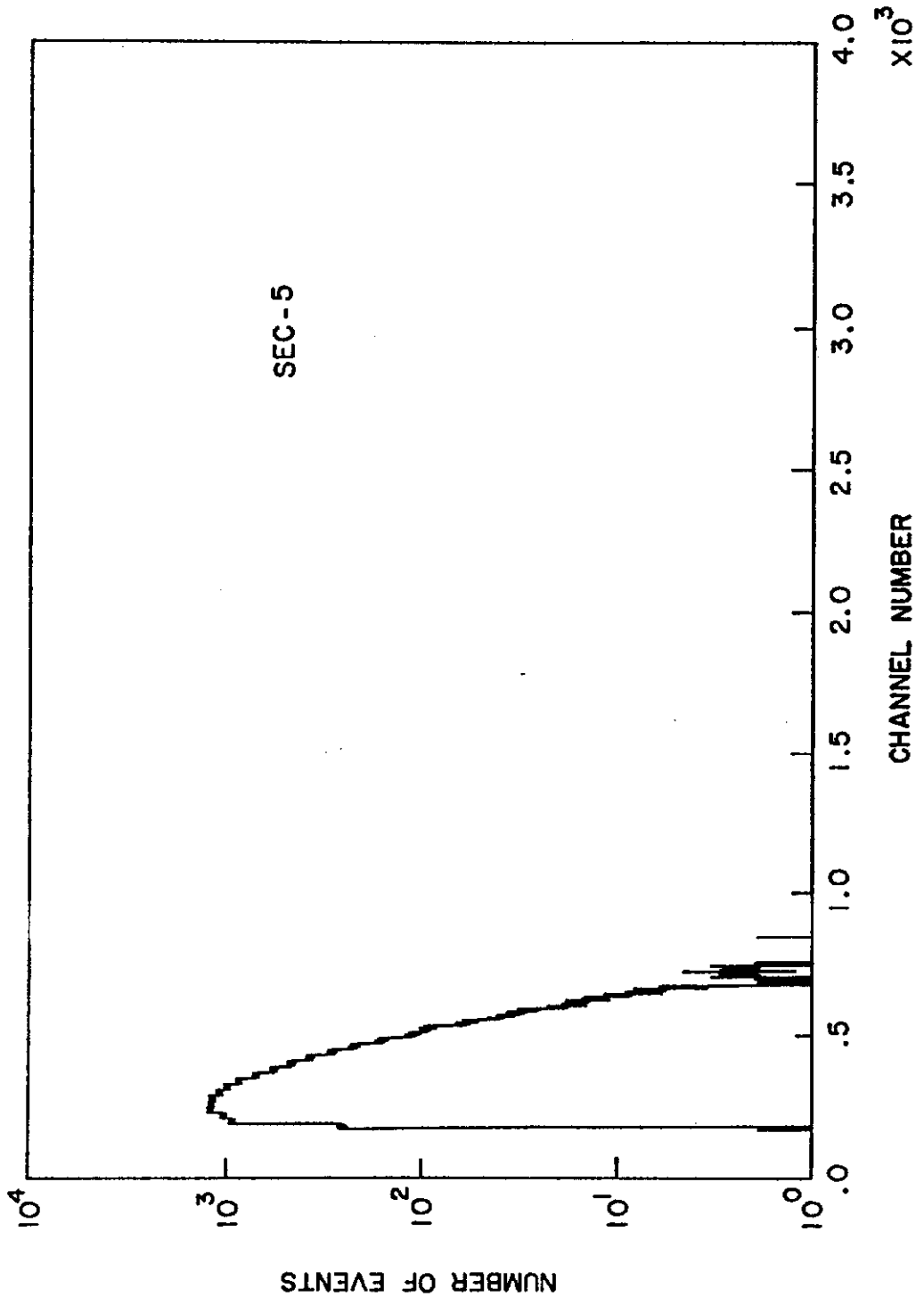
SEC-5
NUMBER OF EVENTS
CHANNEL NUMBER
X10^3
10^0
10^1
10^2
10^3
10^4
.0
.5
1.0
1.5
2.0
2.5
3.0
3.5
4.0

Fig. 17e

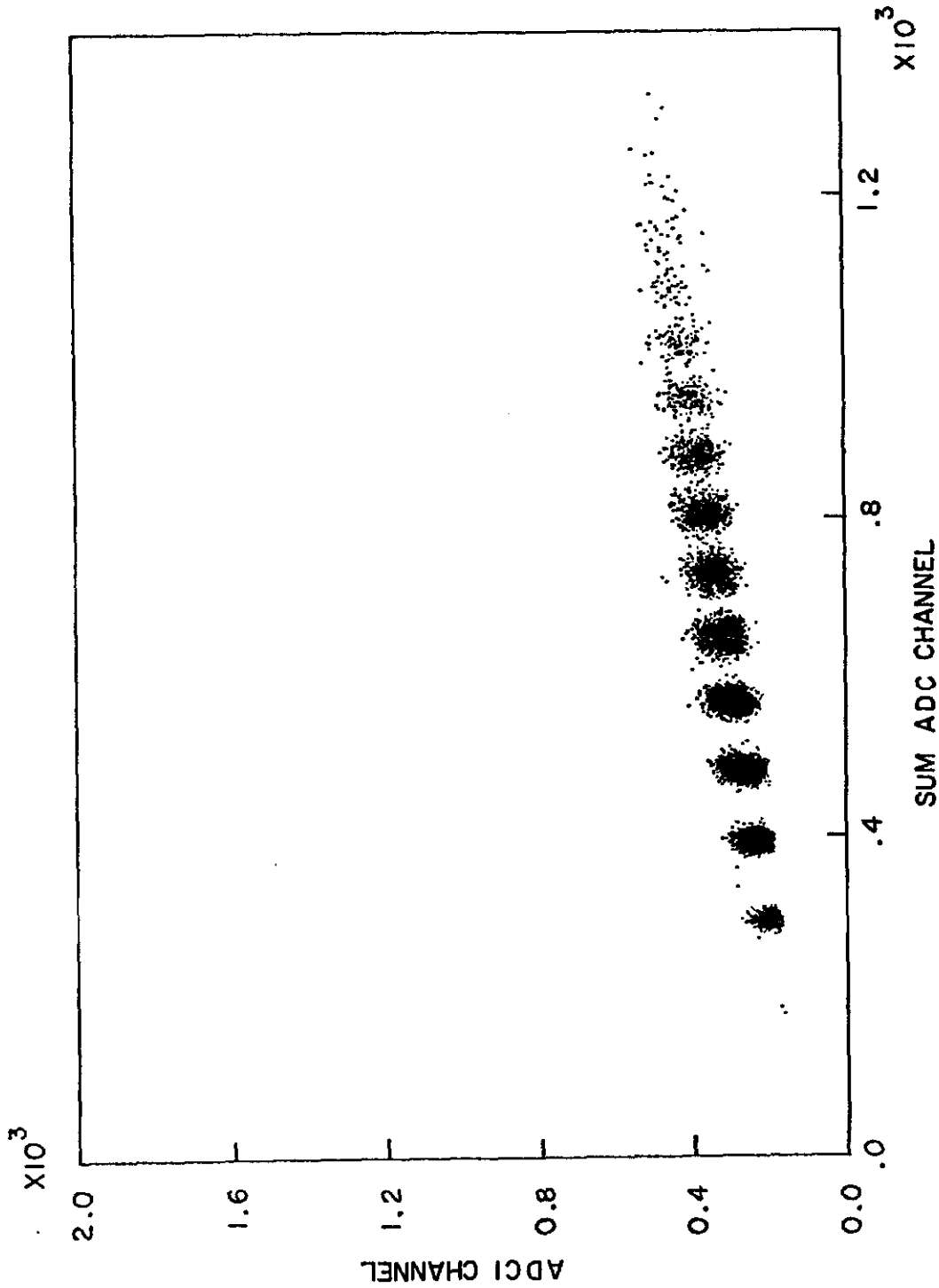

Fig. 18a

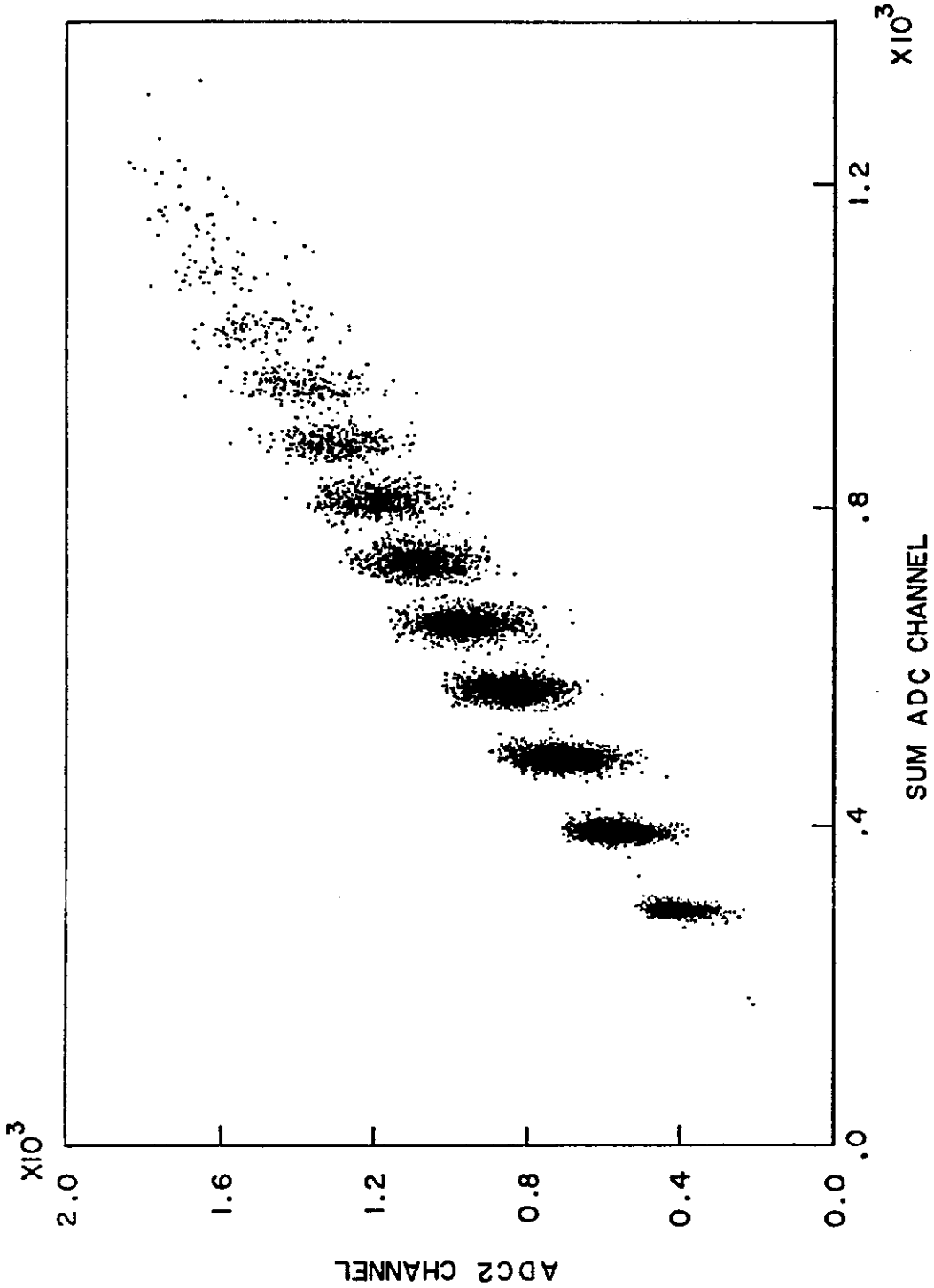

Fig. 18b

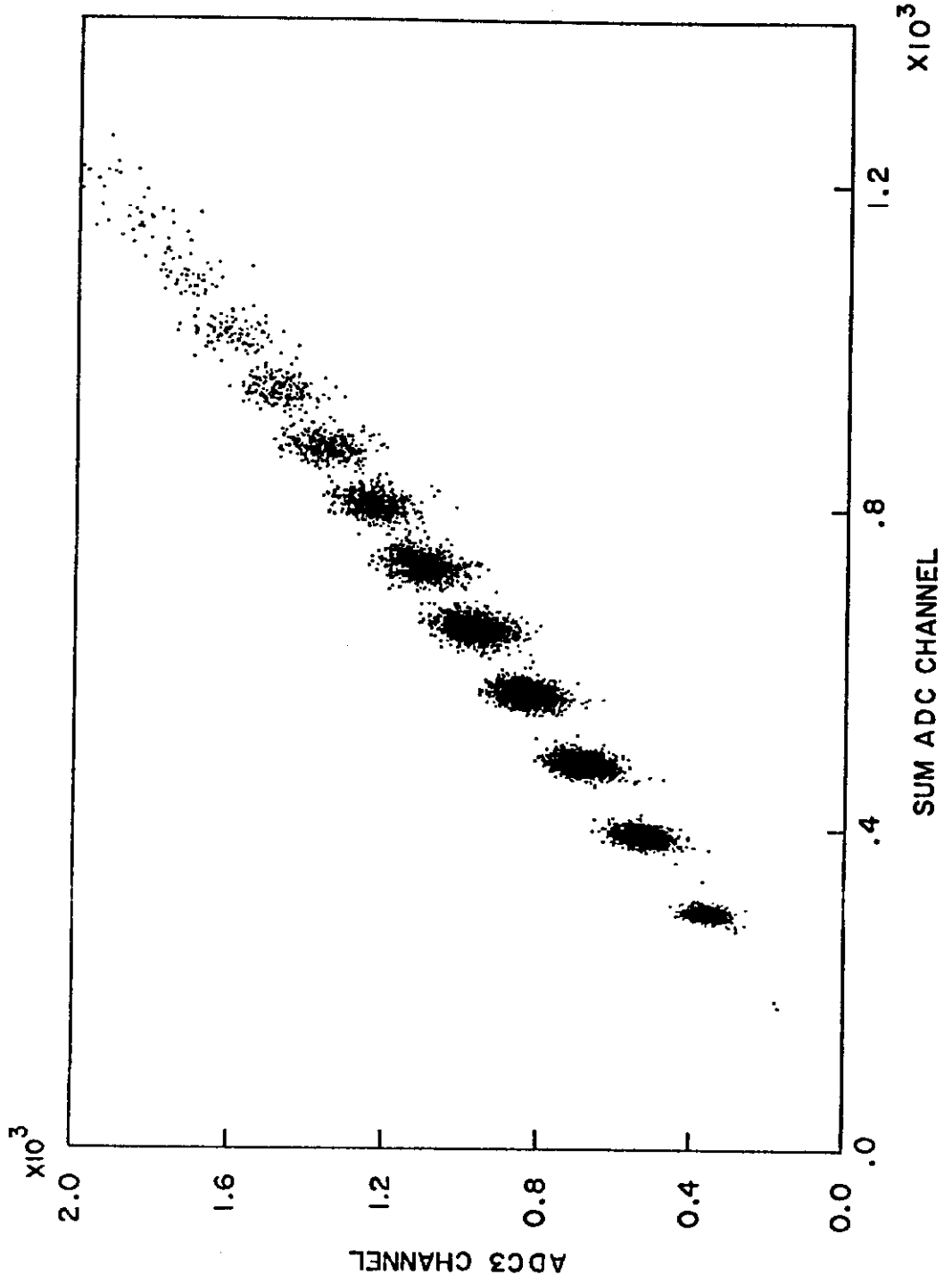

Fig. 18c

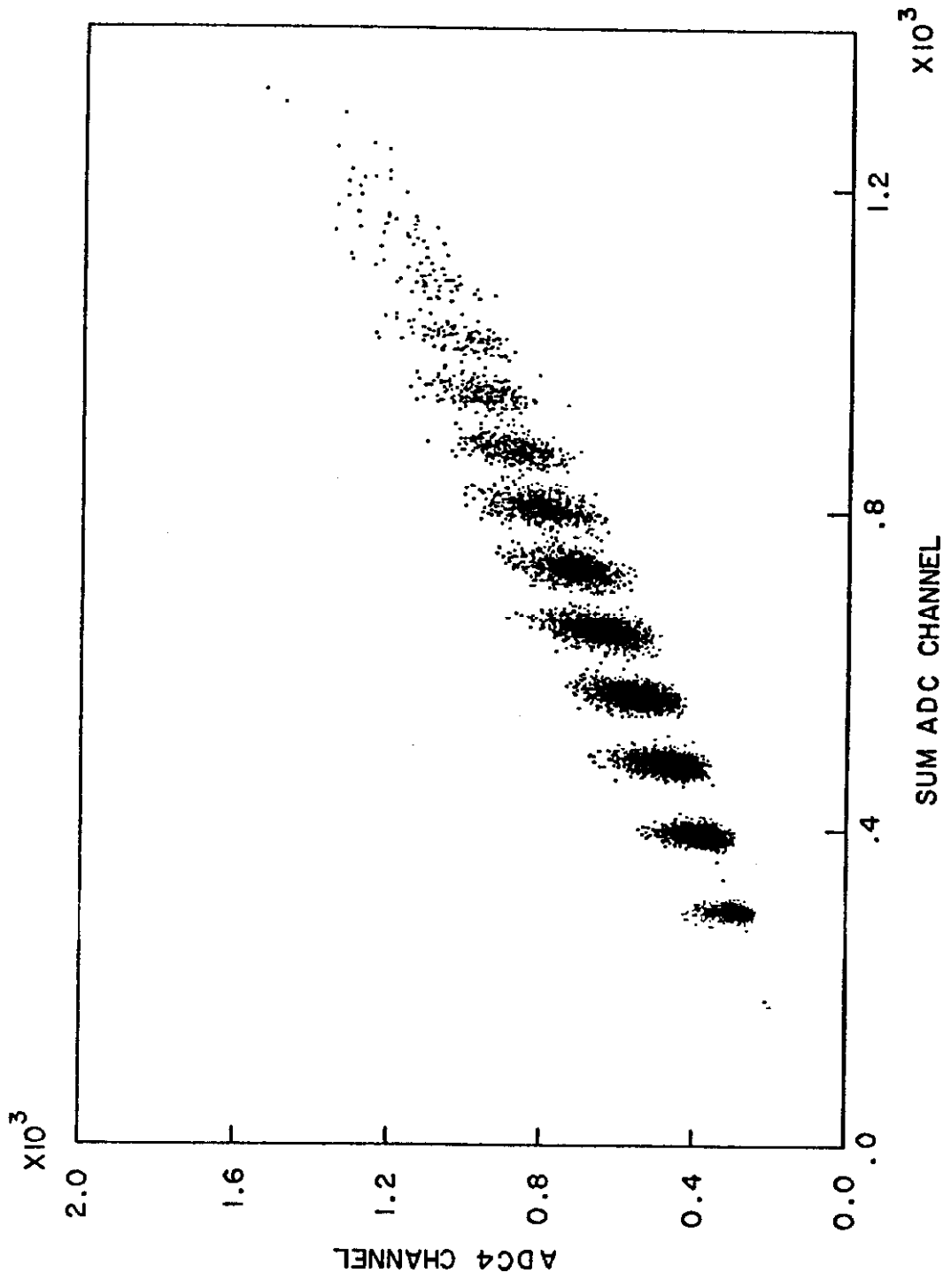
X10^3
2.0
1.6
1.2
0.8
0.4
0.0
ADC4 CHANNEL
0.0
.4
.8
1.2
X10^3
SUM ADC CHANNEL

Fig. 18d

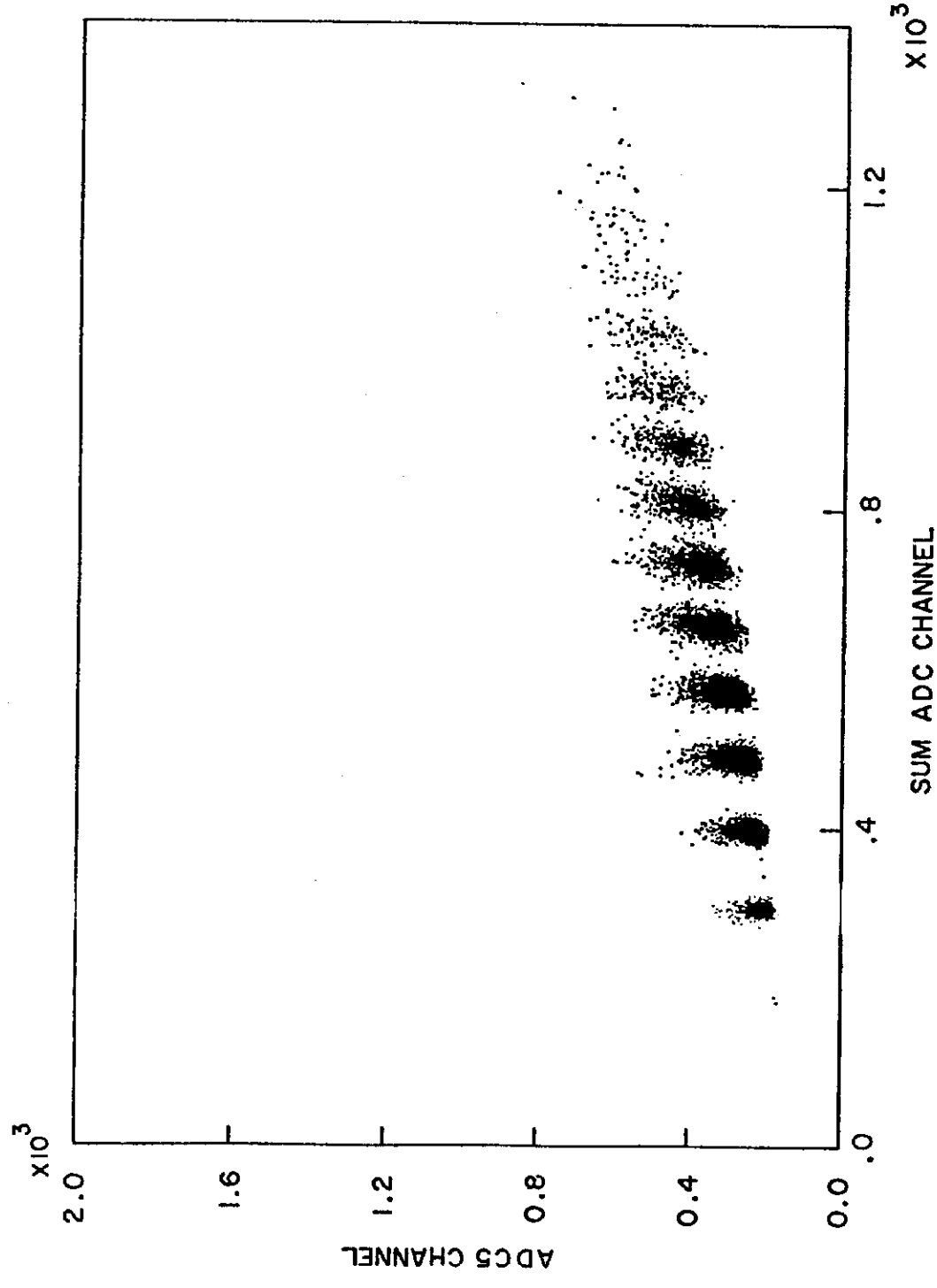

Fig. 18e

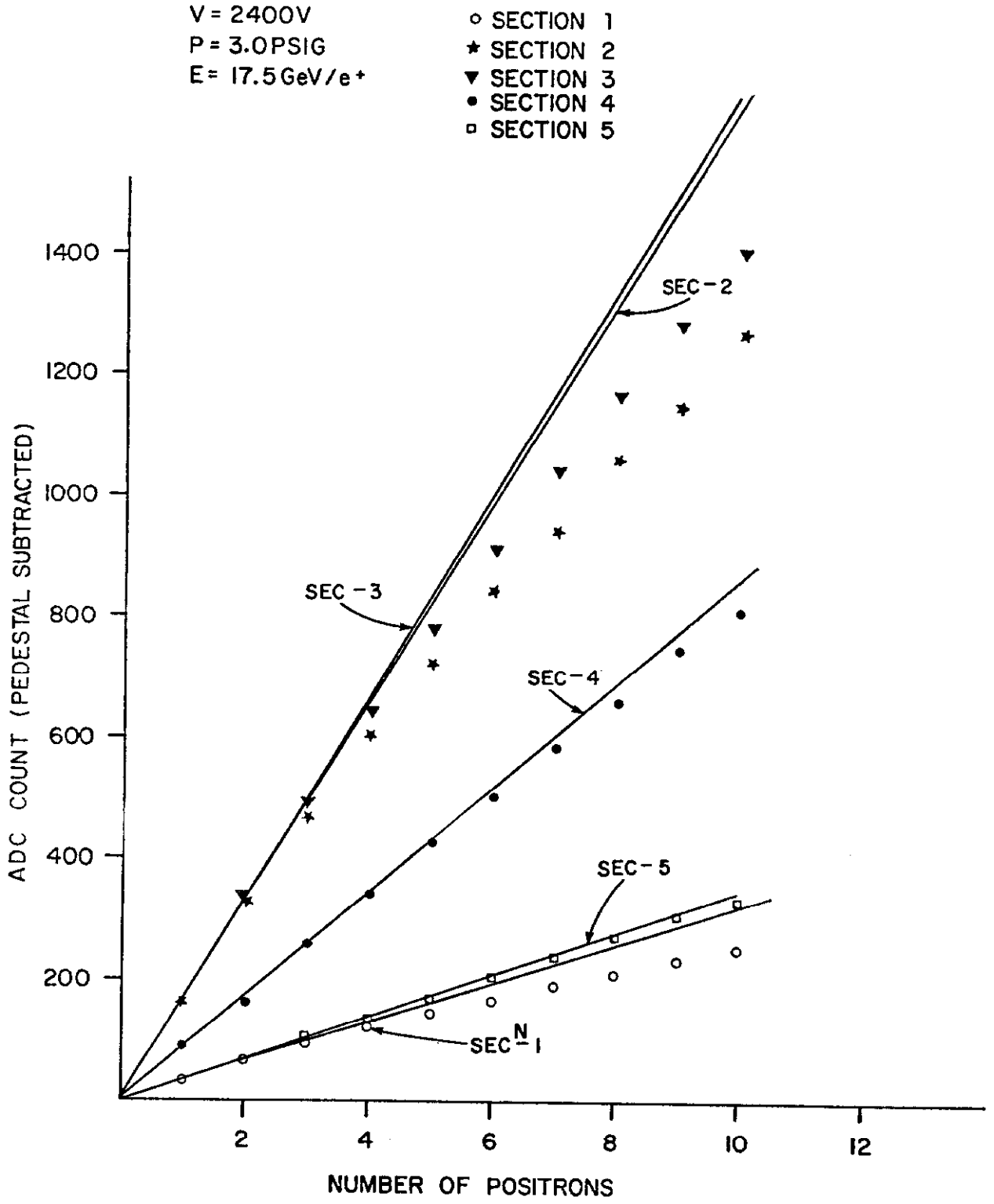
V = 2400V
P = 3.0PSIG
E = 17.5GeV/e+
SECTION 1
SECTION 2
SECTION 3
SECTION 4
SECTION 5
SEC-2
SEC-3
SEC-4
SEC-5
SEC N-1
ADC COUNT (PEDESTAL SUBTRACTED)
1400
1200
1000
800
600
400
200
2
4
6
8
10
12
NUMBER OF POSITRONS

Fig. 19

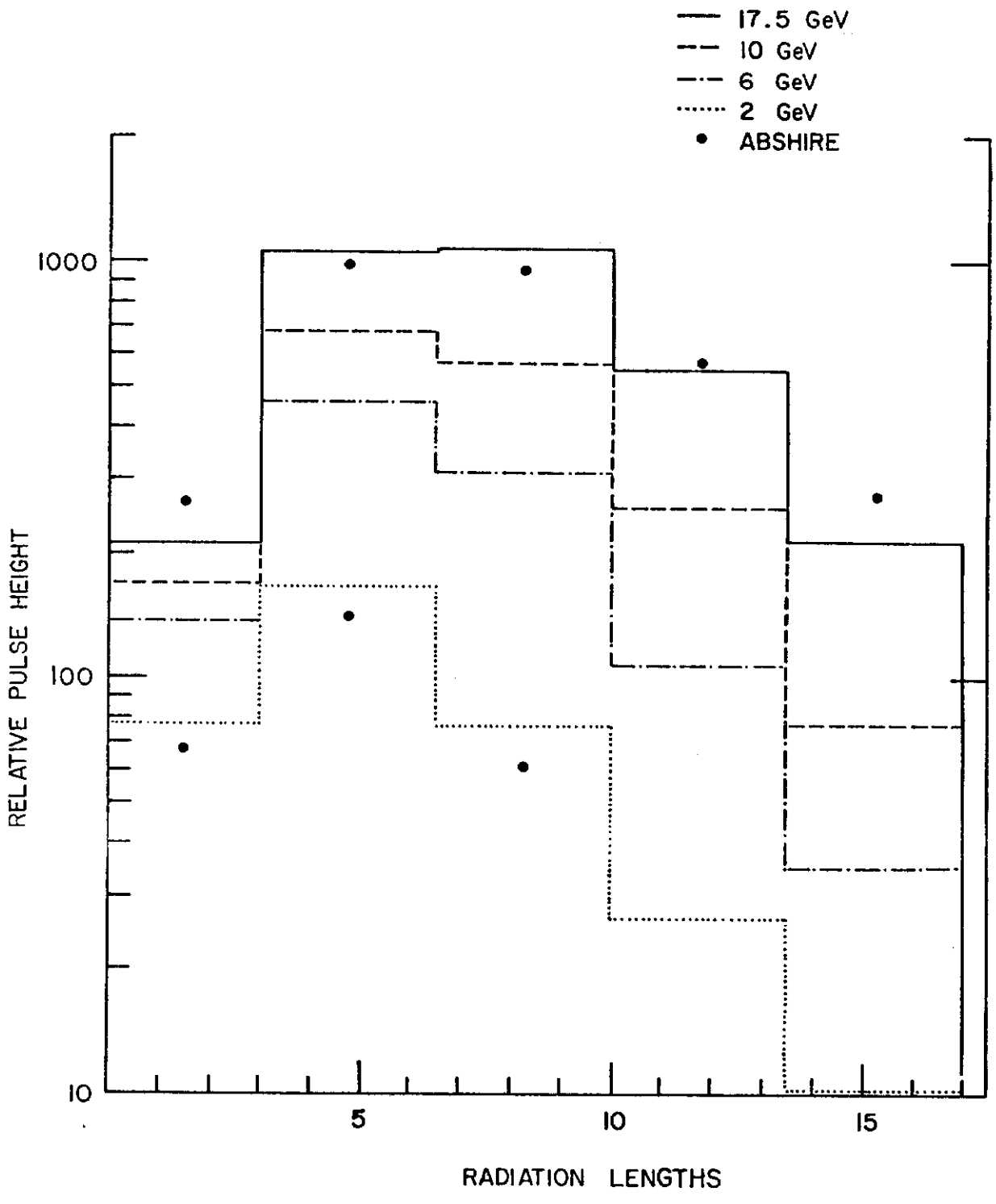
17.5 GeV
10 GeV
6 GeV
2 GeV
ABSHIRE
1000
100
10
RELATIVE PULSE HEIGHT
5
10
15
RADIATION LENGTHS

Fig. 20

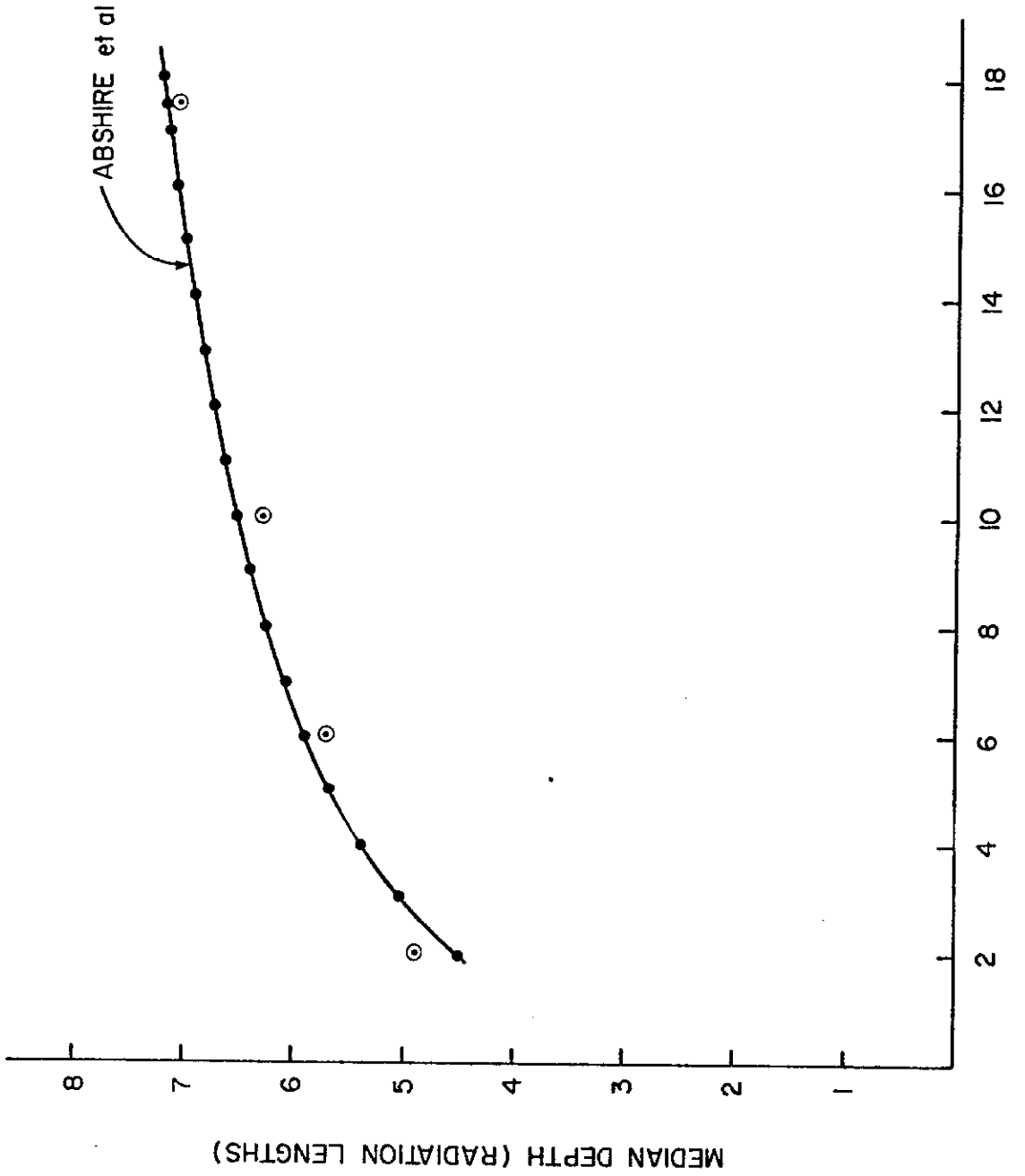
ABSHIRE et al
MEDIAN DEPTH (RADIATION LENGTHS)
INCIDENT ENERGY (GeV)
1
2
3
4
5
6
7
8
2
4
6
8
10
12
14
16
18

Fig. 21

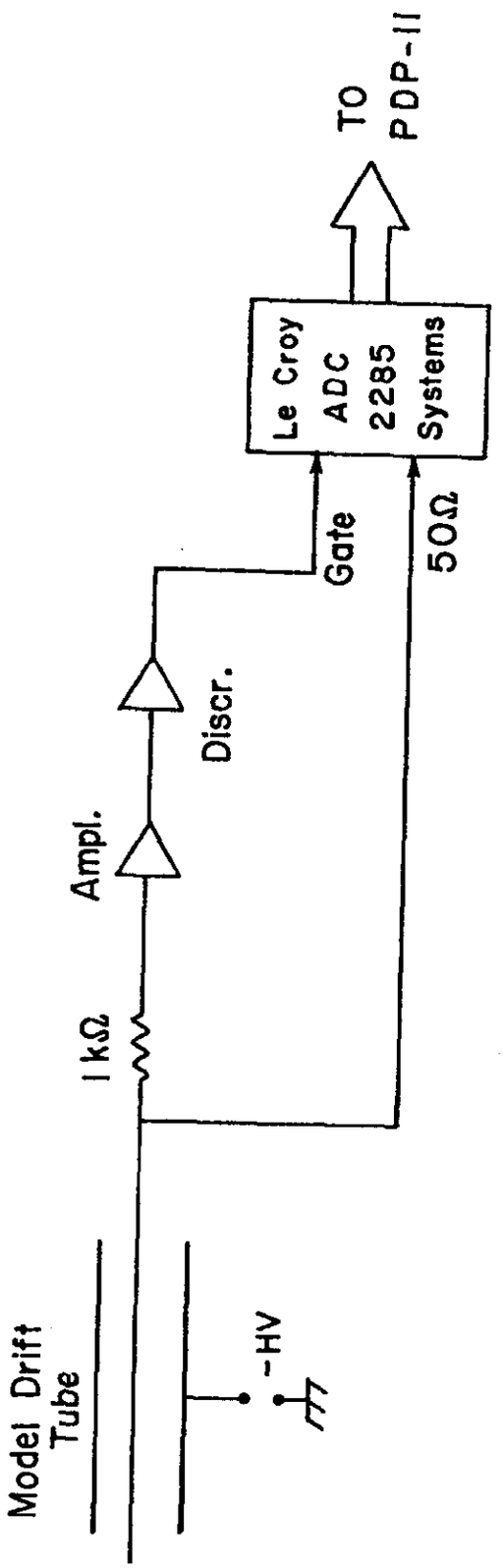
Model Drift Tube
-HV
1 kΩ
Ampl.
Discr.
Gate
50Ω
Le Croy ADC 2285 Systems
TO PDP-11

Fig. 22

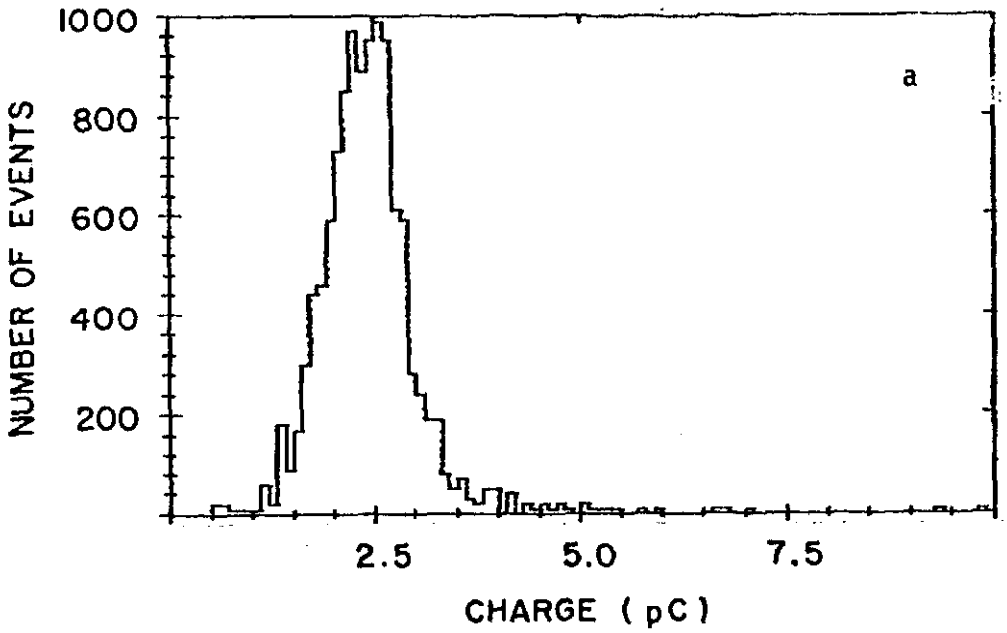

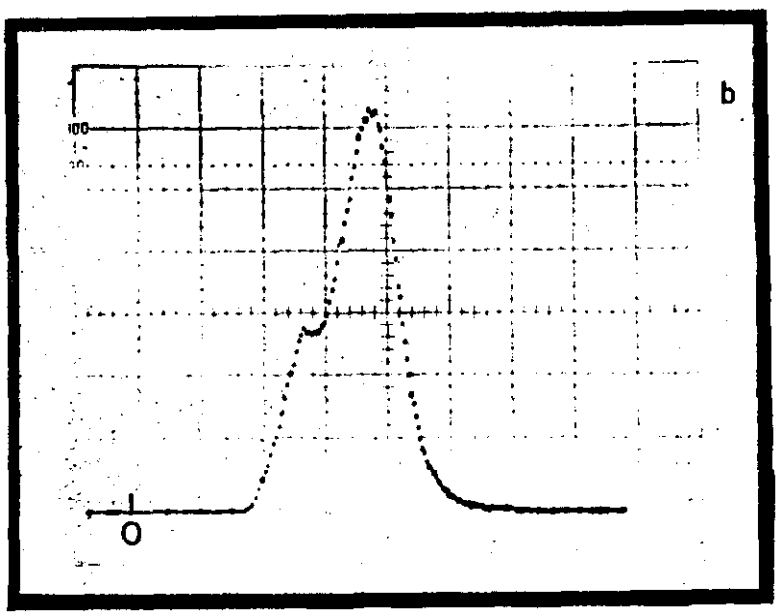

Fig. 23a-b

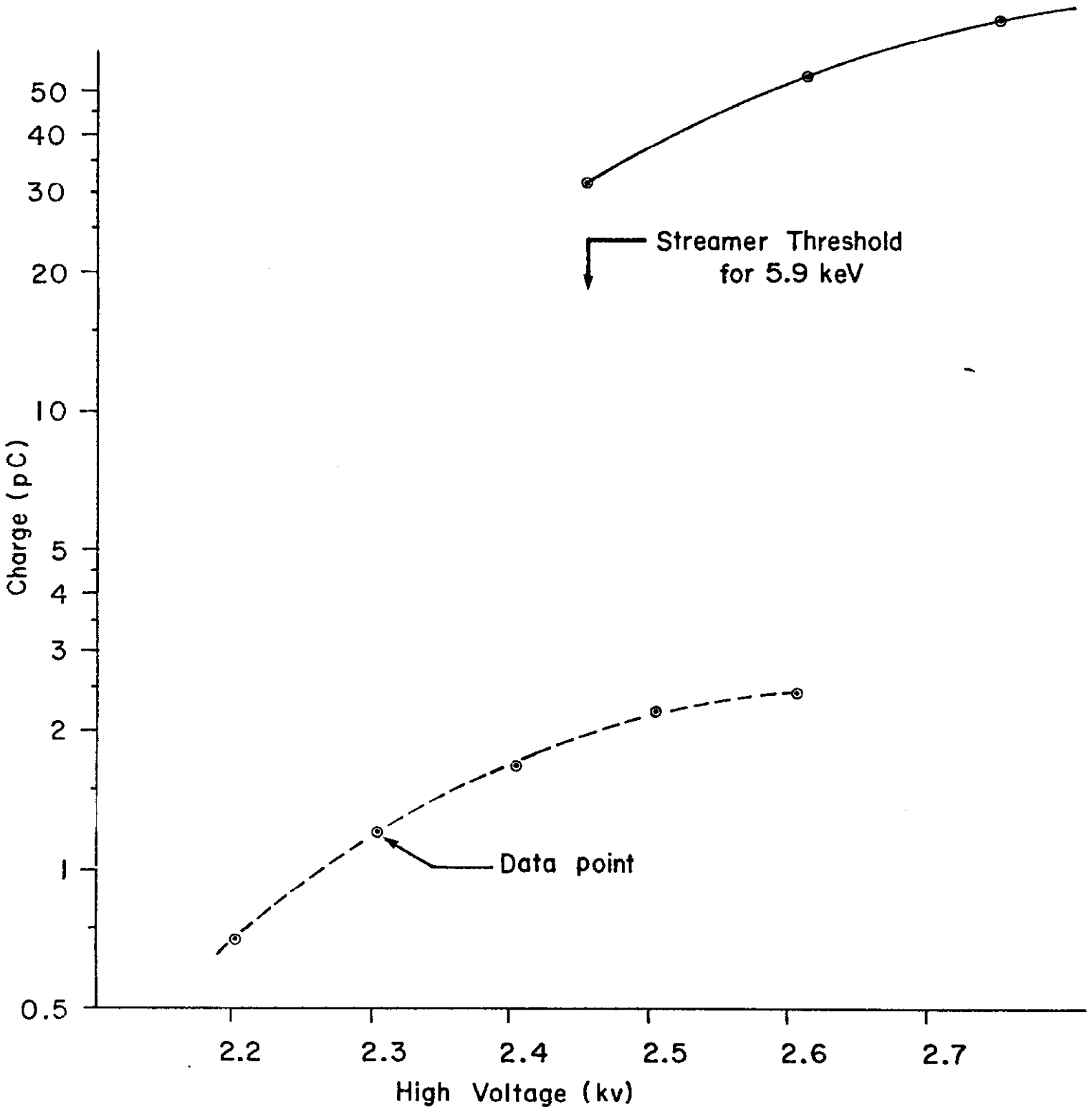
50
40
30
20
10
5
4
3
2
1
0.5
Charge (pC)
Streamer Threshold
for 5.9 keV
Data point
2.2
2.3
2.4
2.5
2.6
2.7
High Voltage (kv)

Fig. 24

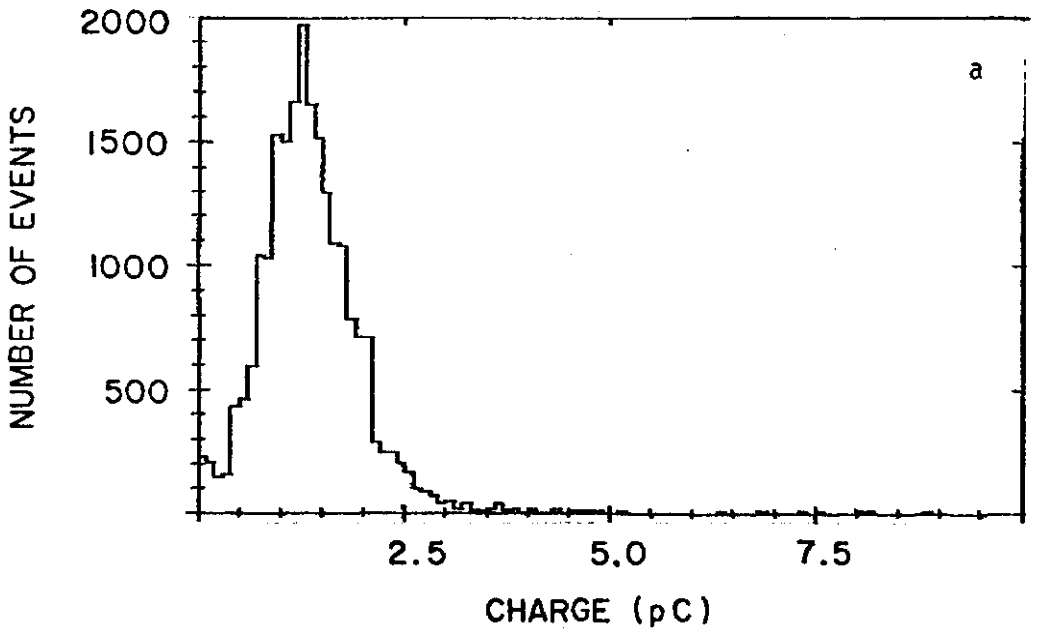
2000
1500
1000
500
NUMBER OF EVENTS
a
2.5
5.0
7.5
CHARGE (pC)

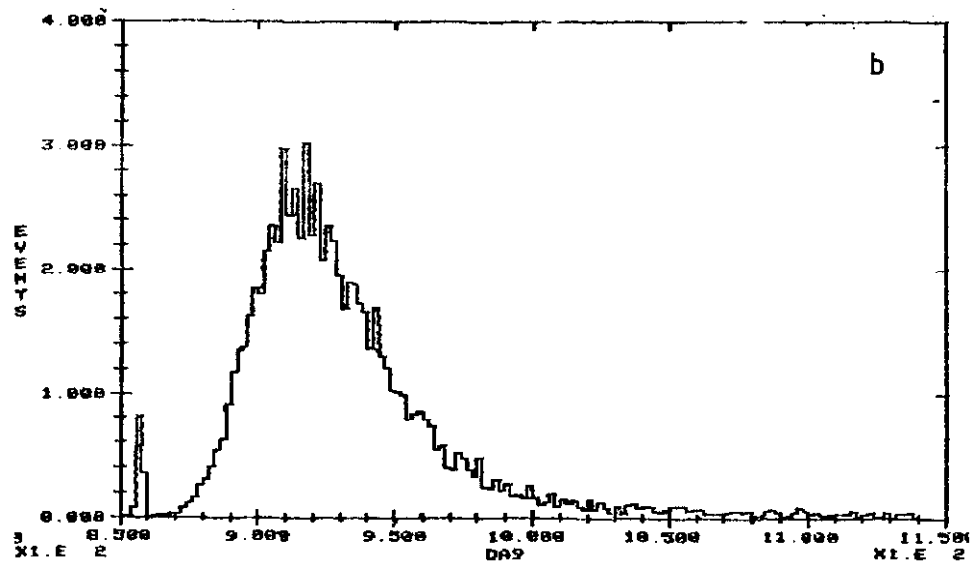
4.000
3.000
2.000
1.000
0.000
EVENTS
b
8.500
9.000
9.500
10.000
10.500
11.000
11.500
X1.E 2
DA9
X1.E 2

Fig. 25a-b